Carbon nanowalls functionalization for efficient O2 reduction catalyzed by laccase using design of experiment

Achraf Blout, Jérôme Pulpytel, Shinsuke Mori, Farzaneh Arefi-Khonsari, Christophe Méthivier, Alain Pailleret, Claude Jolivalt

Carbon nanowalls functionalization for efficient O_2 reduction catalyzed by laccase using Design of Experiment

Achraf Blout[a,b], *Jerome Pulpytel*[b], *Shinsuke Mori*[c], *Farzaneh Arefi-Khonsari*[b], *Christophe Méthivier*[a], *Alain Pailleret*[b], *Claude Jolivalt*[a*]

[a] Sorbonne Université, Faculté de Sciences et Ingénierie, CNRS, Laboratoire de Réactivité de Surface (LRS, UMR 7197), 4 place Jussieu, (case courrier 178), F-75005, Paris, France

[b] Sorbonne Université, Faculté de Sciences et Ingénierie, CNRS, Laboratoire Interfaces et Systèmes Electrochimiques (LISE, UMR 8235), 4 place Jussieu, (case courrier 133), F-75005, Paris, France

[c] Department of Chemical Engineering, Tokyo Institute of Technology, 2-12-1 Ookayama, Meguro-ku, Tokyo 152-8550, Japan

*Corresponding author

claude.jolivalt@sorbonne-universite.fr

Tel: +331 44 27 60 13

Abstract

An enzymatic biofuel cell cathode was elaborated by nano-structuration and functionalization of graphite using two consecutive plasma treatments before immobilization of laccase as a biocatalyst to perform oxygen reduction reaction (ORR) by direct electron transfer ((DET). Nano-structuration of graphite surfaces by synthesis of vertical graphen-like carbon nanowalls (CNWs) was performed by microwave excited plasma enhanced chemical vapor deposition (PECVD). Atmospheric pressure plasma jet (APPJ) system was then used to functionalize chemically the CNWs surface via a rapid and dry route. A partial fractional design evidenced two significant parameters of the APPJ treatment in terms of ORR current density: the treatment time and the inter-distance between the plasma jet and the surface of the carbon material. With the optimized APPJ treatment parameters, a four-fold enhancement of the ORR current density (-440 ± 70 $\mu A/cm^2$) could be obtained on CNWs, compared to graphite electrodes. The maximal current density obtained was about -1 mA/cm^2 with oxidized laccase covalently immobilized on the electrode without any agitation of the solution, confirming the main importance of enzyme orientation on the electrode surface for efficient DET transfer, the relevance of electrode nanostructuration and the advantage of covalent linking of the protein on the electrode surface.

Keywords

Biofuel cell, laccase, atmospheric pressure plasma jet, carbon nanowall, direct electron transfer

Introduction

In the deleterious context for our planet of fossil fuel starvation and green house emissions, fuel cells appear to be an attractive renewable power source provided that its corresponding primary fuel production is decarbonated. Fuel cells generate electricity from the oxidation of a fuel (hydrogen, methanol...) and the reduction of an oxidizer (mostly oxygen). As far as the case of the oxygen reduction is concerned, it is a key reaction for proton exchange membrane fuel cells that is usually catalyzed by platinum, a scarce and expensive metal [1]. An alternative to the use of platinum would be to draw inspiration from the living world and develop fuel cells that do not use any noble metal but rather biological compounds to catalyze the involved reactions. Such devices, whose principle was first established in 1964 by Yahiro *et al.* [2], are called enzymatic biological fuel cells (EBFCs). They are based on a strategy that was shown to be promising for other applications such as biobatteries[3,4] or oxygen sensing[3], which is the use of enzymes as catalysts at the electrodes. In Yahiro's contribution, a hybrid device was designed with an enzyme as catalyst at the anode and platinum at the cathode. Since this proof of concept, major advances have been reported in the design of EBFCs which were reviewed in many outstanding papers, among which some recent ones are cited hereinafter [4-15]. The highest powers reported to date for EBFCs are in the order of mW/cm^2, which makes them suitable for power implantable, wearable or disposable medical devices [16] such as a pacemaker, an artificial urinary sphincter, an ovulation test or a digital thermometer which would thus be autonomous [17-22]. Indeed, biofuel cells are able to generate electricity by transforming glucose or lactate for example at the anode and oxygen at the cathode, two substrates both present in biological fluids. However, many challenges remain to be overcome to optimize EBFCs. For example, most devices using biocatalysts whose substrates are present in living hosts and which were shown to operate at high power density (>1 mW/cm^2) to date actually require the presence of a mediator or a redox polymer to electrochemically wire the enzyme to the electrode [13, 21,

23, 24]. However, such mediators are often toxic and therefore not suitable in the case of implantable devices. Not to mention the diffusion limitations because the mediator must be trapped near the enzyme to be able to commute between the electrodes where it is reduced/oxidized and the active site of the biomolecule [10, 25].

An alternative to the use of redox mediators (or mediated electron transfer (MET)) is to turn to direct electron transfer (DET) which was shown to be possible for enzymes such as bilirubin oxidase and laccase. Indeed, these two enzymes are two multi copper oxidases (MCOs) used as biocatalysts for the ORR at the cathode due to a copper atom close to the enzyme surface. The latter channels the electrons from the reducing substrate to the tri-nuclear cluster at the catalytic center active for oxygen reduction. Currently, in the field of DET-based EBFCs, the research works dedicated to the improvement of their power output and energy efficiency are conducted towards various directions. Among them, one can cite the search for effective methods for enzyme immobilization and optimisation of EBFCs design in order to overcome their known bottlenecks, namely low enzyme loading on the electrode and inefficient electron transfer from the active sites of redox enzymes to the electrode [26]. Interestingly, a hybrid bioelectrochemical system combining an EBFC and a charge-storing component based on cytochrome-c feature was recently reported which enhanced the obtained power density by 15, but compared to the EBFC alone whose power density was less than one $\mu W\ cm^{-2}$ [27].

Numerous materials have been used in academic studies to immobilize MCOs, and especially laccases, as recently reviewed [28]. Among them, carbon materials are an attractive class of materials. They combine many advantages such as high conductivity, relatively low cost, high corrosion resistance in a wide range of potentials and are known for their good biocompatibility which is required when developing an implantable EBFC. More, they can be processed to fabricate different nanostructures such as nanoparticles, nanotubes, graphene,

thus providing a large electroactive specific surface material and a high enzyme loading density, allowing miniaturization of biotechnological devices maintaining high transduction signals [8, 15, 23, 29-35]. Among these materials, carbon nanotubes (CNTs) have been widely used in the development of enzyme immobilization strategies in EBFCs technology in the past ten years, all the more that they are commercialy available and so can be easily used by chemists who are not familiar with material science [36]. CNTs have been deposited on different substrates such as graphite [37], bucky paper [38, 39], or Toray™ carbon paper [40], screen printed electrode[41], even yarn [42] or as the main conductive support for electrodes as agglomerated CNT particles [43, 44] to nanostructure electrodes and enhance their active electrosurface. In the last several years, carbon nanosheets, also refered to as carbon nanowalls (CNWs) have emerged as an alternative type of carbon structure wherein the sharp edged graphene nanoflakes perpendicular to the substrate are distinctive from other carbon structures. These graphene-derivatives are good candidates for catalyst support in fuel cells, conductive electrodes in photovoltaics and energy storage devices such as lithium ion batteries and supercapacitors [45-47] or as far as biofuel cells are concerned, as a graphene-modified graphite cathode in microbial fuel cell to reduce chromium cations (Cr(VI) and thus their toxicity in water[48]). However, CNWs have not been studied to the best of our knowledge as current collectors in an EBFC. CNWs can be readily synthesized using low temperature plasmas including DC, RF and microwave discharges. The main advantage of PECVD when forming vertical graphene nanosheets is the non-catalytic growth process that makes the synthesis possible on any kind of substrates [49, 50]. Besides the interest of high specific surface due to its nanostructuration, carbon is also interesting because of its surface chemical reactivity. This latter allows its surface modification in order to tune its electrostatic or hydrophilic/hydrophobic interactions with the enzyme, leading to improvement of both

loading and orientation of the biocatalyst, thus enhancing the electron transfer from the electrode to the active site of the enzyme [51-54].

Here, we have used an atmospheric pressure plasma jet technique to functionalize graphite and graphene. This method indeed is very advantageous, as it is a rapid, low operating cost and non-polluting process. Plasma techniques have therefore found widespread use for different industrial applications. In particular, atmospheric pressure plasma jets (APPJ) gained large acceptance because they are easy to integrate into existing production lines and they can treat specific parts of a substrate selectively. APPJ treatment has been reported for the functionalization of carbon nanotubes [55-58] mostly for gel-electrolyte supercapacitor applications. In the field of biomolecule immobilization, APPJ was recently used successfully for patterning immobilization of biotin on a vertically aligned CNT microarray with the aim of designing a biosensor [59]. The first attempt to use APPJ for graphite biocathode functionalization with carbonyl and amide/amine groups and subsequent immobilization of laccase was reported in our previous work by Ardhaoui *et al.* in 2013 [60]. N_2 plasma treated graphite electrode led to higher current densities compared to air plasmas but only a few plasma conditions were studied.

Functionalization of the materials used as electrodes in EBFCs is a major concern because it plays an important role in proper orientation of the enzyme and consequently in the direct electron transfer efficiency, knowing that efficient DET relies on intramolecular electron transfer which takes place over less than 1.5 nm, as deduced from quantum mechanical electron transfer concepts[61]. Several studies have highlighted the key role of enzymes (laccase or bilirubin oxidase) orientation on EBFC electrodes [33, 35{Mazurenko, 2016 #766, 53, 62-67] in terms of output power, mainly using adsorption as an enzyme immobilization method. In that case, the immobilization process of the enzyme was shown to be mostly driven by electrostatic interactions, i.e. the zeta potential of the solid on one side, and the

surface charge or dipole moment of the enzyme on the other side. An alternative immobilization method, covalent grafting of the enzyme on surface functional groups, allows to explore additional enzyme orientations resulting from specific bounds formation between functional groups on the surface and amino-acids of the protein. In order to accurately compare both adsorption and covalent bounds formation as immobilization methods while exploring a large set of carbon electrodes with different functional groups properties, we propose here to use an atmospheric pressure plasma jet (APPJ) as the only functionalization method of the carbon surface. Changing the process parameters indeed is likely to tune the resulting density and nature of the surface functional groups of a given material. However, changing variables, one factor at a time, is the typical approach based on a trial-and-error method. This technique, though very informative, is extremely time-consuming [68]. Design of Experiments (DOEs) was thus used, as a structured and organized approach of conducting and analyzing experiments to evaluate the factors that affect the system being studied. Two different graphite morphologies were studied: graphite and graphite electrodes coated with vertical CNWs synthesized by microwave PECVD. Both were functionalized with the same APPJ method, allowing to clearly state about the advantage of enhancing the electroactive surface of the electrode while keeping all other parameters constant. Chemical characterization of the electrodes included SEM, XPS and wettability measurements. After immobilization of a high redox potential fungal laccase from *Trametes versicolor*, the electrodes were characterized by cyclic voltammetry to evaluate the oxygen reduction currents by direct electron transfer. In order to disentangle between the influence of the amount of immobilized enzyme and its orientation, the enzyme surface coverage was calculated from XPS data after laccase immobilization.

2. Experimental Methods

2.1. Chemicals

Laccase from *Trametes versicolor (*activity 400 Unit/mL) was produced and purified according to the method used by T. Bertrand *et al.* [69]. The purified enzyme (with specific activity 300 U/mg) was stored at -20°C in a 10 mM phosphate buffer (PB) solution pH 7.8 containing 15% (w/v) of glycerol. 1-ethyl-3-(3-dimethylaminopropyl) carbodiimide hydrochloride (EDC), N-hydroxysuccinimide (NHS), citric acid and 2,2′-azino-bis(3-ethylbenzothiazoline-6-sulfonic) acid (ABTS) were purchased from Sigma Aldrich. All other products were of analytical grade.

2.2. Elaboration of the electrodes by plasma treatments

The electrodes were prepared from spectrographic graphite rods (diameter 7 mm) purchased from Mersen (France). These latter were cut into 0.2 cm thick graphite disks, then abraded with a SiC paper (P80) during one minute, sonicated successively in distilled water and ethanol and dried using nitrogen prior to their nanostructuration and/or functionalization.

2.3. Experimental setup for graphite surface nanostructuration

Carbon nanowalls were synthetized by plasma enhanced vapor chemical deposition (PEVCD) method described by Mori *et al.* [46]. The microwave plasma-enhanced CVD system used was a modified ASTeX DPA25 plasma applicator in which a quartz discharge tube of a 15 mm inner diameter was utilized. The treatment conditions were as follows: a total flow rate of 50 sccm for CO and 4 sccm for H_2, a working pressure of 250 Pa, a substrate temperature of 700°C and a power of 80 W. The substrate was heated by means of the microwave discharge and its temperature was determined by using an infrared pyrometer (Japan Sensor TMZ9). Three different plama treatment durations were performed (30 s, 60 s and 120 s). According to the processing time, the graphite/CNWs electrodes will be noted graphite/CNWs30s, graphite/CNWs60s and graphite/CNWs120s, respectively They were

characterised using SEM-FEG images that were recorded using an Ultra 55 equipment from Zeiss.

2.4. Experimental setup for graphite functionalization

The APPJ used for this project is manufactured by Plasmatreat GmbH, and consists of a high voltage conical electrode included in a cylinder which acts as a counter electrode (Figure 1). The plasma gas circulates at high flow rate (1000-3000 L/min) in the discharge chamber and the plasma is ignited by means of a high frequency (21 kHz) pulsed DC voltage applied between the two electrodes. The plasma power is supplied by a high voltage generator (PT400® generator, Plasmatreat, GmbH), allowing to control the electrical parameters of the discharge. Current modulation is controlled by means of the Plasma Cycle Time (PCT), which corresponds to the ratio of pulse duration to pause duration. With a PCT of 100%, the pulse duration is equal to the pause duration. The substrate is positioned on a mobile carriage that passes underneath the APPJ, the speed of which ranges from 0 to 50 m/min. The distance between the nozzle and the substrate can also be controlled and is typically between 5 and 15 mm.

Figure 1

2.5. Electrode elaboration

Once functionalization alone using APPJ or the nanostructuration and subsequent functionalization steps using PECVD and APPJ respectively were completed, the graphite disc was mounted as an electrode. To do this, a stripe of copper tape was glued on the entire length of one side of a glass plate (0.8 cm wide and 5 cm long). A drop of liquid indium-galium alloy was deposited on one end of the tape to ensure good electrical contact at the junction with the backside of the graphite disc. The periphery of the graphite disc and the

nearby copper tape are then electrically isolated using a fast drying epoxy resin to seal the graphite electrode (Figure 2).

Figure 2

2.6. Design of experiments (DOE)

Fractional Factorial Design

A 2_{IV}^{4-1} Fractional Factorial Design was used firstly to identify the most important factors that will be investigated more thoroughly with a Central Composite Design. Four factors, namely the plasma cycle time (PCT), the distance between the jet nozzle and the substrate (d), the plasma torch scanning velocity or line speed (V) and the nitrogen flowrate (F), were screened based on their effects on two responses: the water contact angle (WCA) and ORR current density (j) of the biocathode at 0.2 V/SCE. The eight treatments and the corresponding results are listed in Table 3, and each experiment was repeated twice. With a resolution of IV, the main effects are aliased (or confounded) with third order interactions, which allow to estimate the latter correctly, while the 2nd order interactions are aliased with interactions of the same order[70] which makes their estimation not accurate. Therefore, a pure linear model was postulated to explain the results according to Eq. (1):

$$j\ (or\ WCA) = \beta_0 + \beta_1 \cdot PCT + \beta_2 \cdot d + \beta_3 \cdot V + \beta_4 \cdot F + \varepsilon \qquad \text{Eq. (1)}$$

Where β_0 is the mean and β_1 to β_4 are the estimated effects for each corresponding factor. The calculations were perfomed with Matlab 2019. The two most significant factors will then be used to optimize the current density value using a Central Composite Design.

Central Composite Design (CCD)

The response surface methodology (RSM) allows the effects of several factors on a response to be visualized and optimized. Several types of experimental designs are commonly used for this purpose, including the well-known Central Composite Designs proposed by Box and Wilson in 1951[71]. In this second design, the plasma cycle time (PCT) and nitrogen flow rate were kept constant at 80 % and 2000 L/h respectively, which correspond to moderate plasma conditions. The equation of the postulated second order model is as follows:

$$j\ (or\ WCA) = \beta_0 + \beta_2 \cdot d + \beta_3 \cdot V + \beta_{12} \cdot d \cdot V + \beta_{22} \cdot d^2 + \beta_{33} \cdot V^2 + \varepsilon \qquad \text{Eq. (2)}$$

2.7. Surface aldehyde groups quantification

The XPS analysis does not allow to differentiate certain functional groups such as aldehydes, ketones and imines. In our case, this problem arose for the quantification of aldehyde functions. To solve it, aldehydes were chemically derived using a probe molecule. Aldehydes react with hydrazides to form hydrazones whose imine binding can then be reduced to avoid the reverse hydrolysis reaction. The idea was to use a hydrazide as a probe molecule with a characteristic element that can be detected by XPS and unambiguously be assigned to the probe molecule. The probe used was 2-chlorobenzoic hydrazide, which is small in size, thus limiting the risk of steric clutter on the surface of the samples, and which contains chlorine as a probe for XPS. Each graphite disc was immersed in a beaker containing 5 mL of hydrazide solution (0.1 mg/mL) with slight agitation for 4 h at room temperature. 2-chlorobenzoic hydrazide was in large excess compared to the number of aldehyde groups expected to be present on the carbon surface. 50 µL of $NaCNBH_3$ solution (2 mol/L) was then added. The imine reduction took place overnight at 4°C, then rinsed for 5 minutes in ethanol and in water, all under mechanical agitation to remove unreacted hydrazide on the surface.

2.8. Contact angle measurement

The surface wettability was evaluated by measuring the sessile drop contact angle values by a video capture apparatus immediately after plasma treatment with a drop shape analyser (DSA 10 Easydrop, KRÜSS GmbH, Germany). For each measurement, a 1 µL deionized water droplet was dispensed onto the carbon electrode surface and images of water droplet were captured continuously to measure the time resolved water contact angle values. The reported water contact angle (θ (degree)) values corresponded to the average of three measurements, performed on different parts of the samples.

2.9. Laccase covalent immobilization

Laccase was immobilized on functionalized electrodes using two different immobilization methods.

Method 1: laccase was covalently grafted on APPJ functionalized surface via the formation of an amide bond between the carboxylic groups on carbon surface and lysine residues of laccase (scheme 1, amide bond). The carboxylic groups on the electrode surface were first activated with an EDC-NHS mixture. A droplet of an aqueous solution (10 µL) containing NHS (5 mM) and EDC (5 mM) was deposited on the top of the electrode surface and allowed to react during 20 minutes under a glass bell jar. After 20 minutes, the droplet was removed and laccase grafting was performed on the resulting activated electrode: 10 to 15 µL of a diluted laccase (2 U) solution in a 50 mM PB solution (pH=7) was deposited on the electrode surface and allowed to react during 2 hours under a glass bell jar at room temperature. The electrodes were then rinsed under stirring in PB solution during 30 minutes until no laccase activity could be detected in the rinsing solution.

Method 2: it consisted in the formation of an imine bond between the aldehyde groups produced after the oxidation of the glycosylated part of the laccase and the amine groups of the graphite electrodes [67]{Chaga, 1994 #185}[72]. Such method therefore requires a chemical oxidation of the laccase in a preliminary step. This oxidation process was carried out

in two sub-steps. In a first sub-step, the glycerol used for the laccase storage at -18°C was removed by exclusion chromatography using a PD10 (Millipore) column. Then, the purified laccase was oxidized by adding 200 µL of sodium periodate (0.1 M final concentration) during 30 minutes under stirring in the dark. The oxidized laccase was then purified using the same PD10 column to remove the excess of sodium periodate. After this purification step, about 70 % of the activity of the initial laccase was recovered.2 U of oxidized laccase was then deposited on the graphite surface according to the procedure described in Method 1.

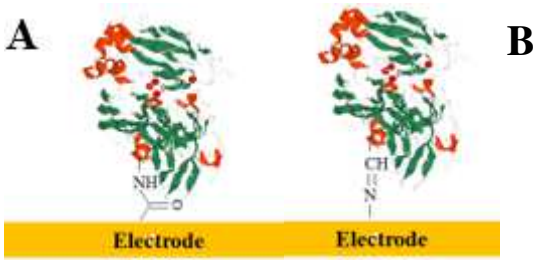

Scheme 1: Schematic representation of the covalent bonds potentially formed on the functionalized carbon surface laccase A) amide bond via a carboxylic group on carbon and a lysine group on lacccase. B) Imine bond via an amine group on carbon and an aldehyde group on an oxidized sugar moity on laccase

2.10. Electrochemical experiments

All ORR-related electrochemical experiments were carried out in acetate buffer (50 mM, pH 4.2) containing 100 mM $NaClO_4$ at room temperature in a conventional three-electrode cell using a Princeton Applied Research Model 263A potentiostat. A platinum wire (Tacussel, France) and a saturated calomel electrode (SCE) reference electrode (Tacussel, France) were used as the counter and reference electrodes, respectively. The solution was sparged for 15 min with pure nitrogen. Nitrogen was kept flowing over the solution during the electrochemical measurements in the absence of oxygen. Cyclic voltammetry response was

recorded between 0.9 and −0.3 V vs. SCE at 10 mV/s. The solution was then oxygenated for 10 min with pure dioxygen before recording ORR current values using the same electrochemical conditions. The faradaic (cathodic) current attributed to biocatalyzed ORR was obtained by subtracting the capacitive current measured at 0.2 V vs. SCE in electrolytic solutions initially de-airated with the help of N_2 bubbling to the global current measured at the same potential in O_2 containing electrolytic solutions.

2.11. Spectroscopic methods

Surface chemical analysis were carried out by XPS, which was performed with an Omicron (ESCA+) X-ray photoelectron spectrometer equipped with a microspot monochromatized Al Kα ($h\nu$ = 1486.6 eV) X-ray source at an accelerating voltage of 14 kV and a current intensity of 20 mA. The base pressure in the experimental chamber was in the low 10^{-9} mbar range. Survey spectra were recorded for the samples in the 0-1.1 keV kinetic energy range with a 1 eV step while high resolution scans with 0.1 eV steps were conducted over the following regions of interest: C1s, O1s, N1s. The values of binding energies (BE, eV) were taken relative to the binding energy of the C1s electrons of sp2 carbon in graphite, which is equal to 284.8 eV. XPS peaks were fitted using CASA software package. The surface composition was determined using the instrument manufacturer's sensitivity factors. The curve fitting process was performed by imposing the peak full width at half maximum (FWHM) of the most resolved peak (C1s sp2 at 284.6 eV) to the other peaks.

3. Results and discussion

3.1. Optimization of the plasma jet functionalization of polished bare graphite

A Plasmatreat atmospheric pressure plasma jet (APPJ) was used to functionalize the surface of graphite electrodes. Several parameters must be set for a given treatment, namely Plasma Cycle Time (PCT), the distance (d, in cm) between the nozzle and the graphite surface, the speed (V, in m/min) at which the jet moves over the graphite surface, nitrogen flow rate (F, in L/h) and finally the voltage pulse frequency. The previous work of Ardhaoui *et al*. [60] performed in our group with the same atmospheric pressure plasma treatment equipment as well as preliminary tests (data not shown) have all enlighted that the use of N_2 as a plasma gas gives better results in terms of current density for ORR than the use of air, all other parameters being constant. Therefore, nitrogen was used exclusively as the plasma gas in this work.

Table 1

APPJ treatment parameters used as a starting point for the statistical analysis design. A pulse frequency of 21 kHz voltage was applied in both cases.

	PCT (%)	d (cm)	Torch velocity (V, m/min)	N_2 flow rate (F, L/h)	Number of treatment passes	Current density ($\mu A/cm^2$)
Preliminary test (this work)	80	1	10	2000	1	53.7±5
From [60]	50	1	15	2400	1	81±8

A graphite sample was treated by APPJ with d=1 cm, V= 10 m/min[1] and F = 2000 L/h and then analyzed by XPS. The functionalization of graphite led to an additional contribution to the C1s signal for binding energy higher than 286 eV, which can be assigned to the presence of oxygenated functional groups on the graphite surface such as C-(O,N) and C=O or even carboxylates around 286.5, 287. 5 and 288.5 eV, respectively (Figure 3) and accounted for around 12 % of the total C1s signal intensity. After decomposition of the C1s peak, the mean value of the carboxylate component ranged between 2 and 3 %.

Figure 3

Biocathodes were then prepared using the plasma functionalized graphite discs by covalent immobilization of laccase using an EDC/NHS mixture as a coupling agent. The measured current density of this biocathode, i.e. the ratio between the O_2 reduction current measured by cyclic voltametry at 0.2 V/SCE to the geometric surface of the electrode (0.38 cm^2) was 53±7 $\mu A/cm^2$. Comparison with the results obtained in our previous work [60] indicate that mild APPJ treatment conditions, i.e. lower PCT and longer distance between the plasma jet nozzle and the substrate, would enhance the performance of the biocathode.

These results were the starting point of our strategy towards improved biocathode performance in terms of oxygen reduction current using DOE. An eight-runs experimental set was first designed to demonstrate the relative significance of the different experimental parameters of the APPJ treatment. Among these, pulse frequency and number of jet passes were kept constant at 21 kHz and 1 pass, respectively, according to the analysis of previous experiments (data not shown) which indicated that these parameters were not significant for dioxygen reduction current values. Therefore, PCT, d, nitrogen flowrate (F) and line speed (V) were the four retained factors. Each of these factors was varied and tested at high (+1) and low (-1) levels (Table 2).

The experimental values of these two levels were determined for each factor (or plasma treatment parameter) according to the following criteria:

- Plasma Cycle Time (PCT): Plasmatreat device makes it possible to produce two very distinct power regimes: a low power regime (PCT between 10 and 50 %) and a high power regime (PCT between 70 and 100 %). Two values were chosen, each representative of one of the regimes (30 % and 80 %).

-The distance d between the nozzle of the APPJ and the substrate allows to control the thermal effect of the plasma on the sample. Preliminary experiments were performed by varying d between 0.5 cm and 2.0 cm with a PCT of 80 %, a line speed of 10 m/min, a flow rate of 2000 L/h and nitrogen as the plasma gas. Contact angle measurements performed on the treated surfaces showed that when d increases, the contact angle increases, i.e. the surface becomes less hydrophilic (Figure 4), which can be detrimental to the catalytic activity of the enzyme which we intend to immobilize on the surface. d = 1 and 1.5 cm were thus set as low and high levels, respectively so that the contact angle remains lower than 50°.

Figure 4

Table 2

Fractional Factorial Design with the experimental conditions and the averaged values of the two replicates for the water contact angle (WCA) and the absolute value of the biocathode current density (j). The coded values for the different factors levels are given in parenthesis.

N°	PCT (%)	d (cm)	V (m/min)	F (L/h)	WCA (°)	|j| (μA/cm^2)
	1	2	3	4 = 123		
1	30 (-1)	1 (-1)	10 (-1)	1000 (-1)	9.7	36.1
2	80 (+1)	1 (-1)	10 (-1)	2000 (+1)	8.4	53.8
3	30 (-1)	1.5 (+1)	10 (-1)	2000 (+1)	55.7	64.8
4	80 (+1)	1.5 (+1)	10 (-1)	1000 (-1)	38.1	63.3
5	30 (-1)	1 (-1)	20 (+1)	2000 (+1)	35.1	79.6

6	80 (+1)	1 (-1)	20 (+1)	1000 (-1)	45.7	82.9
7	30 (-1)	1.5 (+1)	20 (+1)	1000 (-1)	70.9	102.6
8	80 (+1)	1.5 (+1)	20 (+1)	2000 (+1)	68.4	97.5

The above four factors (PCT, d, nitrogen flow F and the torch velocity V) were screened based on their effects on two responses: the water contact angle (WCA) and the current density (|j|) measured for oxygen reduction at 0.2 V/SCE on the biocathode. The analysis of the calculated model parameters (Table 2) shows that the most important factors for controlling the responses are i) the distance between the jet nozzle and the substrate and ii) the torch scanning velocity (treatment time); these factors will then be used to optimize the biocatalytic current density using a Central Composite Design (CCD). It is also interesting to notice that the two responses (WCA and current density) are partially correlated as shown on Figure 5.

Table 3

Estimates of effects and p-value obtained from the 2IV4-1 Factorial Fractional Design. The values of R^2 and of the value of F statistic vs constant model and corresponding p-values are also given for each model. The coefficients with *, ** or *** are statistically significant, at $p < 0.05$, $p < 0.01$ and $p < 0.001$ respectively.

	Water Contact Angle (WCA)		**Biocathode current density, |j| ($\mu A/cm^2$)**	
Parameter	Estimate	p-value	Estimate	p-value
β0	41.5	9.331e-4***	72.57	7.732e-5***
β1	-1.35	0.69597	1.8	0.5041
β2	16.775	0.01278*	9.475	0.02831*
β3	13.525	0.02297*	18.075	0.00472**
β4	0.4	0.906	1.35	0.61
R^2	0.94		0.961	

F-statistic	11.8	0.035*	18.6	0.0186*

Consequently, it appears to be more efficient to have a surface that is not too hydrophilic to obtain a high current (in absolute value). Indeed, the objective of plasma treatment is to create enough polar functions on the surface to be able to subsequently graft enzymes. However, too harsh treatment conditions can damage the surface and lead to the degradation of the current; it is therefore necessary to find a compromise which justifies the use of second order design to optimize the response.

Figure 5

In this second design, the plasma cycle time (PCT) and nitrogen flow rate were kept constant at 80% and 2000 L/h respectively, which correspond to moderate plasma conditions. The experiments performed as a function of i) the distance between the jet nozzle and the substrate and ii) the torch scanning velocity are given in Table 4. The highest current density in absolute value, 115.1 $\mu A/cm^2$, was obtained at a line speed of 42.0 m/min and a distance of 1.6 cm. It should also be noted that, apart from experiments 5 and 9, the measured current densities are quite close to each other regardless of the velocity value and the distance from the jet nozzle to the substrate. This could suggest that the optimization limits of the system have been reached.

Table 4

Composite design for current density optimization. Experimental parameters and the corresponding experimental responses.

Expérience	**d (cm)**	**V (m/min)**	**|j|** ($\mu A.cm^{-2}$)
1	1.2	24.0	104.4
2	1.6	24.0	94.7

3	1.2	42.0	95.9
4	1.6	42.0	115.1
5	1.1	33.0	18.2
6	1.7	33.0	109.7
7	1.4	20.3	97.7
8	1.4	45.7	82.4
9	1.4	33.0	40.7

The results of the linear regression calculated with Matlab are given in Table 5. Unlike the fractional factorial design, the central composite design allows to determine that the interaction between the two factors is relatively strong, even if the p-value is slightly higher than 0.05. The quadratic terms (β22 and β33) are more significant for WCA model as compared to the current one. The CCD results confirm that the WCA and the biocathode current are correlated as shown on Figure 5.

Table 5:

Estimates of effects and p-values obtained from the Central Composite Design. The values of R^2 and of the value of F statistic vs constant model and corresponding p-value are also given for each model. The coefficients with *,** or *** are statistically significant, at $p < 0.05$, $p < 0.01$ and $p < 0.001$ respectively.

	Water Contact Angle (WCA)		**Biocathode current density |j| ($\mu A/cm^2$)**	
Parameter	Estimate	p-value	Estimate	p-value
β0	46.99	0.00507**	86.7	0.0048**
β2	26.48	0.00130**	14.6	0.0273*
β3	-7.817	0.0398*	-5.59	0.263
β23	9.187	0.0625	15.97	0.069

β22	8.370	0.109	-1.55	0.832
β33	7.107	0.152	3.99	0.595
R^2	0.982		0.899	
F-statistic	33.1	0.00792**	5.37	0.0986

Figure 6

Figure 6 compares the experimental values of the ORR biocatalytic current densities with those calculated from the polynomial model whose parameters were determined using the central composite experimental design. We observe that some points are well predicted by the model, with a relative gap between 1 and 6% (highest jet nozzle to substrate distance) whereas for the lowest jet nozzle/substrate distances tested, the prediction is less accurate. More, for jet nozzle/substrate distances higher than 1.4 cm, the current density varies only slightly with the operating conditions of the plasma functionalization. This area can be described as robust.

By plotting the contours of the current response surface as shown in Figure 6, it is possible to determine an optimal region for plasma functionalization to be performed. However, the nature of the functionalized groups on the surface is critical for the immobilization method to be used.

In order to identify the functional groups on the surface of graphite samples after their APPJ functionalization, XPS analysis was carried out. After decomposition, the two highest contributions were centered at 284.6 eV and 285.4 eV, encounting for 72.7% and 17.6% of the total intensity respectively, can be assigned to sp^2 and sp^3 hybridization of C-C or C-H bonds, respectively [14]. Additional peaks can be assigned to C-O and C=O (286.2 eV, 5.6 % of the total carbon content and 287.5 eV, 2.9 %, respectively). No peak was observed between

288 and 289 eV, the binding energy characteristic of carboxylic groups. This result was confirmed for all treated surfaces with d higher than 1.2 cm.

As the peak at 287.5 eV assigned to carbonyl cannot however discriminate between ketones or aldehyde groups, an attempt was therefore made to identify and quantify the aldehyde functional group density using a chemical probe. The latter was 2-chlorobenzoic hydrazide which reacts with surface aldehyde groups, if any, and forms a hydrazine group which can be detected by XPS thanks to the presence of a chlorine contribution, originating only from the probe molecule. Figure 7 shows the high resolution Cl2p peak of the plasma-functionalized graphite after reaction with 2-chlorobenzoic hydrazide. One can observe on Figure 7, the characteristic spin orbit splitting at 200.6 eV binding energy for Cl2p1/2 eV, assigned to organic chlorine[73], thus confirming the presence of aldehyde groups on the graphite after APPJ treatment. The surface density of chlorine calculated from XPS data therefore allows to quantify the aldehyde group density on graphite, supposing that all surface aldehyde groups reacted with 2-chlorobenzoic hydrazide which was in excess as compared to aldehyde groups (Table 6).

Figure 7

Table 6

Surface aldehyde group densities after APPJ treatment of bare graphite, calculated with electrode geometric surface (0.38 cm^2).

d (cm)	V (m/min)	I_{Cl2p}/I_{C1s}	nCl2p ($\times 10^{-9}$ mol/cm^2)
1.6	24	0.0467	6.25
1.4	20,3	0.0396	5.22
1.5	20	0.0387	4.90
1.6	42	0.0370	4.52
1	10	0.0459	6.08

The calculated chlorine densities using the geometric surface of the graphite sample are higher than those expected for a dense monolayer, as a result of the obvious underestimation of the specific area that is likely to be larger than the geometric area as our graphite electrodes show a rather rough surface [65]. Even if they were not accurately quantified, the aldehyde groups were nevertheless clearly evidenced on plasma treated graphite electrodes, which can influence the subsequent laccase immobilization process. Indeed, they could lead to the spontaneous Schiff base formation , i.e. a covalent imine bond with lysine residues of laccase and thus contribute to the immobilization of the enzyme on the surface functionalized with the optimal plasma conditions determined thanks to the composite design. Laccase covalent immobilization could thus proceed via the lysine groups of the protein and two different type of functional groups on carbon surface: carboxylic groups and/or aldehydes ones, the latter option being rarely studied in the field of bioelectrodes development.

In conclusion, the use of the composite experimental design identified five experimental conditions for the APPJ treatment of graphite in which catalytic currents greater than 95 $\mu A/cm^2$ were obtained. Mild APPJ treatment conditions appear to be favorable to enhance the biocatalytic current density measured for ORR. We therefore chose to work in the so-called robust zone and test these conditions on graphite electrodes nanostructured with carbon nanowalls.

3.2. Carbon nanowalls electrodes

3.2.1. CNW synthesis

A low-pressure Plasma Enhanced Chemical Vapor Deposition in a CO/H_2 microwave discharge system was used to deposit carbon nanowalls (CNWs) [46] on graphite electrodes. At the optimum CO/H_2 feed ratio of 46 sccm/4 sccm, resulting carbon nanowalls showing a thickness of several tens of nanometers were synthetized and then analyzed using scanning

electron microscopy (SEM). An extremely high growth rate of 1 μm.min^{-1} was reached in our system with a relatively low microwave discharge power of 60 W for a substrate growth area of 1 cm^2.

Carbon nanowalls were organized as free-standing nanosheets. They form an assembly of inter-twinned walls. It can be observed from Figure 8 that the increase in the treatment time has the effect of increasing the density of CNWs. Thus, for a deposition time of 30 s (Figure 8a), the graphite surface was not completely covered by the nanowalls. Subsequently, the nanowalls formed with a processing time of 30 s were not further used in the present work. CNWs deposited for longer treatment times i.e. 60 s and 120 s (subsequently referred to as graphite@CNWs60s and graphite@CNWs120s, respectively) were used for the nanostructuring of the graphite substrate. For a 120 s process, CNWs were thinner and denser, however, the sheet-like structure of CNWs was still discernible. The deposits were spherical in shape, as seen in Figure 8d).

Figure 8

The results of XPS analyses based on the decomposition of the C1s photoelectron peak and perfomed on a graphite@CNWs60s and graphite@CNWs120s surface (see Figure 9a) are shown on Table 7. A slight increase in the Csp^3/Csp^2 ratio was observed when the duration of synthesis of the CNWs also increased. This observation is in line with the results obtained by S. Mori *et al.* with Raman spectroscopy showing that the graphite crystallinity decreased with the growth of CNWs [46].

Table 7

C1s decomposition X-ray photoelectron spectra of bare graphite@CNWs60s and graphite@CNWs120s supports.

	C1s			**O1s**	**O/C**	**N1s**
	C sp^2	**C sp^3**	Csp^3/Csp^2			

graphite@CNWs60s	74	16.5	0.22	2	0.022	-
graphite@CNWs120s	70,2	18	0.25	1.9	0.021	-

Due to the nanostructuration of the graphite surface, the available surface for further enzyme immobilization was obviously increased compared to bare graphite. However, as the objective was to increase the biocatalytic current, the electrochemical active surface area (EASA) was also investigated (see part S1 of supplementary information). For graphite@CNW60s and graphite@CNW120s, EASA was estimated to 0.18 and 0.25 cm^2, respectively, i.e. lower than the pristine graphite geometrical surface: 0.38 cm^2. It was hypothesized that such a discrepancy could result from the poor hydrophilicity of the CNW surface (only 2 % dioxygen from the O/C ratio determined from XPS mesurements, and no nitrogen). EASA was thus also determined on graphite@CNW60s functionalized with APPJ (O/C 0.15). As expected, EASA was higher: 1.21 cm^2, i.e. 3.2 times larger than the geometric surface. Such an EASA enhancement compared to the geometric surface dimension remains modest but is in line (even higher) with the one measured for CNW formed by soaking a graphite substrate in liquid nitrogen and exhibiting CNWs whose topography is very similar to the one obtained in the present work [48].

3.2.2. APPJ functionalization of graphite@CNW electrodes

Graphite@CNWs60s and graphite@CNWs120s samples were functionalized with APPJ treatment using optimized conditions deduced from CCD on "bare" graphite surfaces (see Table 10). For comparison purposes, graphite/CNWs samples were also processed according to harsh APPJ parameters, i.e. d=1 cm and V= 10 m/min. In the latter case, the XPS analysis (Table 9 and Figure 9b) showed that surface atomic composition is very similar whatever the duration of CNWs synthesis. The ratio N/C was very low, around 1 %, but significant,

showing that the plasma functionalization induced the formation of nitrogen containing functional groups on the surface since no nitrogen was detected on bare CNWs. Functionalization by APPJ mostly introduced oxygenated groups on CNWs since the O/C ratio increased from 0.022 for bare CNWs to 0.15 for treated CNWs, (Tables 7 and 8). C1s peak decomposition indicates that 8.1 % and 5.8 % of the overall amount of carbon atoms are involved in C-O bonds and carbonyl ones, respectively, for harsh plasma treatment conditions. Carboxylic groups account for about 3 % of the overall carbon content, which corresponds to a surface concentration of around 10 atoms per nm^2, i.e. a rather high value compared to the surface concentration of a close-packed monolayer (8 molecules per nm^2 for phenyl for example[74]).

However, when using mild plasma functionalization conditions, XPS analysis showed that there is no significant component around 288-289 eV in the C1s peak, thus excluding the presence of carboxylic groups on the functionalized nanowalls surface for all the optimized processing conditions. Similar results were found on bare graphite samples.

Table 8

XPS analysis of graphite/carbon nanowalls samples after APPJ treatment and calculated COOH surface density. Plasma treatment parameters: d= 1 cm; V=10 m/min; Flowrate = 2000 L/h; PCT: 80 %.; one cycle.

Binding energy (eV)	**284.6**	**285.4**	**286.3**	**287.2**	**288.4**	**O/C**	**N/C**	**Csp^3/ Csp^2**	**COOH density ($atoms/nm^2$)**
Composition	**C sp^2**	**C sp^3**	**C-O**	**C=O**	**COOH**				
graphite@CNWs60s	66.5	16.3	8.1	5.8	3.0	0.15	$8.6.10^{-3}$	0.24	10.2
graphite@CNWs120s	65.8	15.7	8.6	7.0	2.9	0.15	0.011	0.23	9.9

3.2.2. Laccase immobilization on functionalized CNWs

Subsequently to the graphite@CNWs functionalization, laccase was immobilized on the samples. Two immobilization conditions, with or without EDC/NHS mixture as a coupling agent, were tested for the ORR current density. The EDC/NHS solution, which is likely to enable the formation of a covalent bond between carboxylic and amine groups, was used to activate the carbon support and rinsed before deposition of laccase solution. In such conditions, an amide bond formed only via the carboxylic groups available on the electrode, if any, i.e. after functionalization in harsh conditions (d = 1 cm and V = 10 m/min). Nevertheless, EDC/NHS mixture was used also for the support functionalized in mild plasma conditions for comparison purposes. The current intensity measurments were all performed at pH 4.2, also for comparison purpose with literature in the field of laccase biocathodes.

Table 9:

APPJ treatment parameters and bioelectrocatalytic performances of graphite@CNWs biocathodes after APPJ functionalization and laccase immobilization in the presence of EDC/NHS.

N°	d (cm)	V (m/min)	|j| (µA/cm^2) on graphite@CNWs60s	|j| (µA/cm^2) on graphite@CNWs120s
1	1.6	24.0	440± 70	337 ± 37
2	1.4	20.3	369± 41	380 ± 32
3	1.5	20.0	216± 18	426 ± 57
4	1.6	42.0	277± 27	332 ± 48
5	1.0	10.0	201±17	433 ± 21

The highest current density (440±70 µA/cm^2 in absolute value) was measured on graphite@CNWs60s functionalized with the following plasma processing conditions: nozzle

to substrate distance = 1.6 cm, an APPJ velocity = 24 m/min (Table 9), more than twice the current density obtained with much harsher conditions i.e. d= 1 cm and V= 10 m/min which lead to a current density of 201±17 $\mu A/cm^2$ (in absolute value). A similar enhancement was observed for bare graphite electrodes, for which the ORR current density (in absolute value) increased from 53.7±5 to more than 94.7 $\mu A/cm^2$ This result emphasizes that the optimum parameters determined thanks to the CCD on bare graphite are also relevant for graphite@CNW60s electrodes. From a molecular point of view, the current density enhancement observed when shifting from harsh to mild plasma conditions however can not be explained by different laccase immobilization features. For harsh conditions, XPS analysis showed that carboxylic groups were observed on functionalized graphite@CNWs60s (Table 8), so that amide bonds can be formed between the electrode surface and the amine group of lysine residues of the enzyme (see scheme 2). In mild conditions, oxydation of graphite is less advanced so that only aldehyde groups are formed on nanostructured graphite, which are likely to form spontaneously imine bonds with amine groups of laccase (see imine 1 on scheme 2). For both types of covalent bondings, the orientation of the enzyme on the electrode is similar since the same laccase residues are involved, namely lysine ones. It could be assumed that the highest current density observed for mild conditions compared to harsh ones could therefore result from a higher amount of active laccase when immobilized on graphite@CNWs60s *via* an imine bond formation.

When graphite@CNWs120s electrodes were tested, two different couples of parameters used during APPJ plasma treatment (distance, in cm and velocity in m/min), i.e. 1.5 ;20 and 1 ;10 both led to similar current density values: 426±57 and 433±21 $\mu A/cm^2$ (in absolute value), respectively. Obviously, the optimized APPJ plasma processing conditions through the implementation of an experimental design did not lead to any current enhancement. It is noteworthy to mention that the obtained current density was similar to the best ones obtained

for graphite@CNWs60s, 440±70 µA/cm^2 (in absolute value), although this latter current density value was obtained under slightly different plasma processing conditions. All the plasma functionalization conditions tested on graphite@CNWs120s electrodes presented in Table 9 resulted in a mean current density value of 383 µA/cm^2 (in absolute value), with a standard deviation of 47 µA/cm^2 , a value very similar to the one resulting from repeatability measurements. It can therefore be concluded that for graphite@CNWs120s electrodes, the selected plasma conditions were within a robust area.

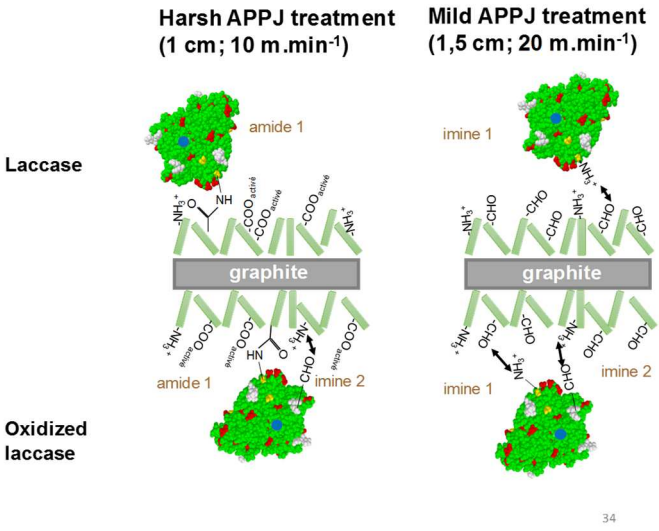

Scheme 2: Covalent immobilization of laccase on the nanostructured and functionalized graphite surfaces. Laccase representation has been drawn using Rasmol 2.5 software using the tridimensional structural data of the protein deposited in the Protein Data Bank (1KYA). Accessible surface atoms are shown as balls of different colours: Lysine residues of laccase appear in yellow, glycosilation moities in white and aspartic/glutamic residues in red. Blue balls stand for the copper atom of T1 catalytic center.

In order to get further insight into laccase immobilization process, the influence of the presence of the coupling agents EDC/NHS mixture was checked with graphite@CNWs120s electrodes leading to the highest current densities measured at that point, namely those recorded for two differents sets of parameters during plasma functionalization: d=1; V=10 and

d=1.5; V=20. In the absence of EDC/NHS, the obtained current densities values were 273 ± 9 and 315 ± 19 µA/cm^2 (in absolute value), respectively (**Fig**ure S2). Knowing that the current density measured for the same functionalisation conditions in the presence of EDC/NHS are respectively 433±21 and 426±57 µA/cm^2 (in absolute value), it can therefore be concluded that the current density was significantly higher in the presence of EDC/NHS. In harsh finctionalisation conditions, carboxylic groups are formed at the electrode surface, so that the presence of EDC/NHS allows their activation and leads to the formation of an amide bond with amine groups of lysine residues of laccase. Such covalent bonds tightly tether the enzyme on the surface, thus reducing a potential leaching, all the more likely to take place that both enzyme (whose isoelectric point is 3) and CNWs funtionalized with carboxylic groups are negatively charged at the pH value used for the immobilization process.

To summarize the results related to ORR current density, a maximum value around 440 µA/cm^2 was observed with both graphite@CNW60s and graphite@CNW120s electrodes, i.e. a four times higher current density than on bare graphite in optimized plasma conditions for the functionalization of the surface. Compared to what could be expected based on the increase of the specific area of the graphite electrode due to the deposition of carbon nanowalls, the result was somewhat deceiving and prompted us to turn to further improvements.

Previous studies performed in our group have shown that high bioelectrocatalytic currents were obtained when oxidized laccase was used [65]. Interestingly, the group of Di Bari has also used oxidized laccase to prepare graphene based-biocathodes as a mean to orientate the enzyme before its covalent bonding by formation of amide bonds by carbodiimide coupling[35, 75]. Oxidation of laccase intends to target glycosidic groups resulting from postraductional modifications of the protein. Fungal laccases are indeed glycosilated enzymes whose sugar moities are involved in the stabilization process against proteolysis (four

glycosilation sites were evidenced in the crystal structure of the laccase from *T. versicolor* used in the present work[76]. We took advantage of this laccase property to perform the oxidation of polysaccharide residues in glycosilated laccase with sodium periodate, thus providing an efficient way of generating aldehyde groups for subsequent conjugaison with amine containing functionalized carbon support. More precisely, a Schiff base can be formed between aldehyde groups of the enzyme and amine groups on the support[77]. This technique is widely used to covalently graft antibodies for biosensor development for example[72] or grafting of enzymes[78, 79]. We therefore compared the performances of functionalized graphite@CNW60s electrodes coated with either natural or oxidized laccase. In both cases, nitrogen was used as the plasma gas with a gas flow rate of 2000 L/h and a PCT of 80%. One experiment was performed with a nozzle/substrate distance of 1 cm and a line speed of 10 m/min, i.e. in harsh plasma conditions, and the second one with d= 1.6 cm and V=24 $m.min^{-1}$ which are representative of mild conditions. These latter provided the highest current density values on graphite/CNWs60s electrodes after oxidized laccase immobilization. However, it was observed for a given set of plasma treatment conditions, that the current densities were only slightly higher for oxidized laccase. It can therefore be assumed that on graphite@CNW60s, the expected imine bond formation between the oxidized glycosidic groups of the enzyme and surface amine groups of CNWs (imine 2 on scheme 2) had no significant influence on the laccase bioelectrocatalytic activity.

Figure 10

With graphite@CNWs120s supports however, it could be observed that the immobilization of the oxidized laccase resulted in better catalytic currents than that of the non-oxidized enzyme for given plasma parameters or immobilization procedure (see Figure 10). The highest measured current density corresponding to ORR was was 956±86 $\mu A/cm^2$ (in absolute value) with electrodes treated with APPJ plasma at a distance of 1 cm and a line speed of 10

m/min on which oxidized laccase was covalently immobilized by amide bonds thanks to the presence of EDC/NHS as activation agent during the immobilization procedure. In addition, the imine bond formation with oxidized laccase significantly increased the biocatalytic activity of the enzyme since, for all tested immobilization conditions, the ORR current density was higher with oxidized laccase compared to unmodified laccase. Two hypotheses could support this result: first an increase in the amount of immobilized enzyme and second a better wiring of the redox protein allowing a direct electron transfert. Indeed, three out of the four glycosidic moieties of laccase are located on the same side as the Cu T1 copper site cleft. A multipoint attachment of the protein via these groups would thus favor the electron transfert by minimizing the distance between T1 center and the electrode while stabilizing the enzyme position on the surface. Interestingly, it can be noticed that the optimal current density obtained in the present work is very similar to the one reported by Di Bari et coll. in 2016 for graphene based biocathode with oxidized laccase grafted by carbodiimide coupling[35]. The authors also emphasized the anchoring role of the interaction between amino-aryl layer and the aldehyde groups of oxidized laccase. In the research field focused on orientated immobilization of laccase, it should be mentioned that recent papers whose strategy was based on non-covalent immobilization of laccase through hydrophobic interactions likely to take place in the vicinity of the T1 acive site have reported dioxygen current as high as 2.4 mA/cm^2 using a bifunctional anthroquinone/amadantane linker and more recently 3 mA/cm^2 with a mutant laccase bearing an unique lysine residue near the T1 active site and covalently immobilized on CNT by a linker including β-cyclodextrin-modified gold NPs[52, 67, 80-82]. The currents density reported in the present work remains thus competitive with the best results in the literature, while obtained with an original strategy of surface nanostructuration. Instead of deposited graphene or CNT on bare carbon, we propose to form CNWs firmly

attached to the carbon substrate and to functionalize the carbon by a rapid APPJ method, thus avoiding the use of additional linkers.

In addition, as enzyme orientation on the surface is not the only parameter likely to affect the current density, we propose to correlate the latter results to the amount of enzyme immobilized on the support by quantifying the laccase immobilized on the electrode surface using XPS data. Indeed, a clear modification of the C1s peak was observed after laccase covalent immobilization step on graphite@CNWs electrodes that undubitably evidenced enzyme immobilization. Notably, a very significant enhancement of the carboxylic and carbon-nitrogen (or -oxygen, C-N(or -O)) contributions at 288.5 eV and 286.6 eV respectively, was observed (Figure 9c) compared to the spectrum obtained for the graphite@CNWs120s electrodes functionalized with the same APPJ parameters before laccase immobilization (Figure 9b).

However, the presence of an amide signal at 287.5 eV on both functionalized electrodes made it difficult to unravel accurately the contributions of the enzyme and the graphite, respectively from XPS analysis. Consequently, it was chosen to focuse on the copper signal for a quantitative analysis of the protein coverage rate. Copper indeed is present only in laccase, so that its corresponding signal can be unambiguously assigned (see Figure S3 for an example of a Cu XPS spectrum obtained with oxidized laccase immobilized in the presence of EDC/NHS). The quantitative analysis of laccase coverage rates from the XPS signal relies on comparison of the experimental I_{Cu}/I_{C1s} signal intensity ratios calculated from experimental values with the ratios calculated using one of the two following models of discontinuous laccase layers. The related model for laccase coverage assumes that the geometry of immobilized enzyme is a hemisphere with a diameter d_{enzyme} and leads to the following expression for I_{Cu}/I_{C1s} ratio (equation 4) [83]:

$$\frac{I_{Cu}}{I_{C1s}} = \frac{\gamma.n_{Cu}^{enzyme}.\sigma_{Cu}.T(E_{Cu}).\lambda_{Cu}^{enzyme}.[1-\Lambda]}{\gamma.n_{C1s}^{CNW}.\sigma_{C1s}.T(E_{C1s}).\lambda_{C1s}^{CNW}.\Lambda+(1-\gamma).n_{C1s}^{CNW}.\sigma_{C1s}.T(E_{C1s}).\lambda_{C1s}^{CNW}+\gamma.n_{C1s}^{enzyme}.\sigma_{C1s}.T(E_{C1s}).\lambda_{C1s}^{enzyme}.[1-\Lambda]} \quad \text{(Eq. 4)}$$

where Λ, the attenuation factor of the signal due to the presence of the enzyme layer can be calculated as follows:

$$\Lambda = \left(\frac{8\lambda^2}{d_{enzyme}^2}\right)\left[1-\left(\frac{d_{enzyme}}{2\lambda}+1\right)\exp\left(-\frac{d_{enzyme}}{2\lambda}\right)\right] \quad \text{(Eq. 5)}$$

where γ stands for the fraction of the surface covered by a protein layer, n_{Cu}^{enzyme}, n_{C1s}^{enzyme}, n_{C1s}^{CNW} are the concentrations of Cu or C (subscript) in the enzyme (superscript enzyme) or in the CNWs covered substrate (superscript CNWs). The latter concentration was calculated from the ratio of the volumetric weight to molar weight, with $\rho_{CNx}=\rho_{graphite}=2.1$ g/cm^3. For laccase, the concentration of an element S was calculated as follows:

$$n_S^{enzyme} = \frac{\rho_{enzyme} \times N_S^{enzyme}}{M_W^{enzyme}} \quad \text{(Eq. 6)}$$

With $\rho_{enzyme}=1.4$ g/cm^3. The number of carbon atoms of one laccase molecule is the sum of the carbon atoms of the primary structure, i.e. 2399 (knowing that the formula of the peptidic chain of laccase is $C_{2399}H_{3600}N_{638}O_{729}S_9$) and the carbon atoms from the glycosidic part of the protein which accounts for a molecular weight of 9588 Da, assuming that the four sugar chains evidenced on the protein structure according to the crystallographic data [84] are formed by 2 N-acetyl glucosamines and 11 mannoses each, they would include 328 carbons, leading to a total number of carbon atoms N_C^{enzyme} equal to 2727.

σ_{Cu} and σ_{C1s} are the photo-ionization cross sections for nitrogen and carbon, respectively. $T(E_{Cu})$ and $T(E_{C1s})$ are sensitivity factors provided by the instrument manufacturer.

The products $\sigma \times T(E)$ are 63.5 and 1 for copper and carbon, respectively.

λ_{Cu}^{enzyme} (1.5 nm), λ_{C1s}^{CNx} (3.3 nm) and λ_{C1s}^{enzyme} (3.3 nm) are inelastic mean free paths of Cu2p electrons through the enzyme layer and of C1s electrons through carbon and the enzyme, respectively. θ is the take-off angle, i.e. the angle between the surface normal and the axis of the analyzer lens ($\cos\theta = 0.7$).

As mentioned above, the intensity of the copper signal was chosen as being the most relevant indicator of laccase because this element was only present in the enzyme. Consequently, I_{Cu} can be expressed as only one term standing for the copper signal from the enzyme. Calculations were performed with the two characteristic dimensions (d_{enzyme} parameter) of the protein, i.e. 5 nm and 7 nm, based on the crystal structure of the enzyme [76, 85]. The intensity of the carbon signal, I_C, is described as the sum of three terms (i) carbon signal from graphite/CNWs recovered by a fraction γ of enzyme layer, (ii) carbon signal from uncovered (1-γ) graphite/CNWs and (iii) carbon signal from the enzyme.

Table 10 summarizes the results. Coverage rates were calculated assuming that the laccase adopts a hemispherical shape on the electrode surface. Indeed, a previous work in our group[65] has shown that a model of a flat enzyme layer is almost not sensitive to the dimension of the enzyme. d_{enzyme} whereas, by using a hemispheric model however, Γ is systematically higher for d_{enzyme}= 5 nm than for d_{enzyme}=7 nm, as expected.

Table 10:

Laccase coverage rate Γ on graphite@CNWs120s electrodes calculated with ratio ICu/IC1s from XPS experiments. Laccase was immobilized in the presence of EDC/NHS.

	APPJ treatment conditions		
	d = 1 cm and V = 10 m/min	**d = 1.5 cm and V = 20 m/min**	
	Oxidized laccase	**Natural laccase**	**Oxidized laccase**
d_{enzyme} = 5 nm	0.5	0.4	0.8
d_{enzyme} = 7 nm	0.4	0.5	1

The laccase coverage rates calculated from the ICu/IC1s ratio in case of mild plasma treatement conditions evidenced that the amount of immobilized oxidized laccase is twice that of the unmodified one, i.e. 0.8 as compared to 0.4, respectively. As the experimental ORR current also doubled, these two results could be correlated, thus confirming the above hypothesis of a more efficient laccase immobilization on graphite@CNWs120s support. Unfortunately, for harsh plasma treatment condition, the copper signal was too low to be detected for samples with unmodified laccase, so that this conclusion could not be confirmed. However, the absence of copper signal indicates that the amount of immobilized non-oxidized laccase is low. With oxidized laccase, a laccase coverage around 0.4 could be calculated. Also not fully quantitative, these results are in line with those observed for mild plasma conditions. Another conclusion from our experimental results is that a higher amount of immobilized enzyme does not translate directly, into a higher ORR current density. The orientation of the enzyme should also be taken into account since the highest current density (956±86 $\mu A/cm^2$ in absolute value) was measured for a low surface coverage of oxidized laccase.

4. Conclusion

In the present work, we used graphite as starting electrode material which was covered with graphene-like carbon nanowalls entangled in a vertical position. The surface of the substrate was thus nanostructured, which considerably increased its specific area. Plasma enhanced Chemical Vapor Deposition (PECVD) was used to synthetize the carbon nanowalls using a mixture of carbon monoxide and dihydrogen as the plasma. Then the carbon nanowalls were functionalized by means of atmospheric pressure plasma jet in nitrogen. In order to optimize the plasma functionalization conditions, a series of experimental designs were carried out. As the number of samples were limited, it was decided to carry out the

optimization study on bare graphite substrate (without carbon nanowalls) as a preliminary step. First, a fractional experimental design was performed to determine experimental parameters of APPJ (nozzle-substrate distance, nozzle velocity, PCT and plasma gas flow) which influence the performance of graphite electrodes in terms of current densities measured for ORR. It was pointed out that the distance and velocity of the APPJ were the most significant parameters which influence the performance of the laccase modified graphite electrodes. Subsequently, it was decided to carry out a central composite design (still on graphite electrodes) in order to optimize the plasma functionalization parameters. This experimental design made it possible to reach current densities in the range of 95 to 105 $\mu A/cm^2$ (in absolute value) and to identify a so-called robust zone for APPJ treatment conditions. It should be noted that only aldehyde groups were formed as a result of milder treatment conditions, thus limiting the oxidation process of graphene. Experiments using graphite/CNWs60s and graphite/CNWs120s electrodes for the above optimal APPJ treatment conditions allowed to reach cathodic current densities of 440 ± 70 $\mu A/cm^2$ with graphite/CNWs60s, thus evidencing that the optimized conditions determined with the central composite design on bare graphite electrodes were appropriate to graphite/CNWs60s nanostructured surfaces as well. The presence of nanowalls on the graphite surface has therefore increased the bioelectrocatalytic current density by a factor of 4.4 compared to the one measured on bare graphite functionalized with the same optimal APPJ treatment parameters. The comparison between natural and oxidized laccase was also performed for several types of immobilization, namely adsorption or covalent grafting, i.e. with or without coupling agent. The maximum current density obtained was about -1 mA/cm^2 for plasma-treated graphite/CNWs120s electrode at a nozzle-substrate distance of 1 cm, a PCT of 80%, a flow rate of 2000 L/h and a line speed of 10 m/min with oxidized laccase covalently immobilized. The results underline that a higher amount of immobilized laccase (as quantified

from XPS data) did not translate inevitably into an increased biocatalytic current, thus confirming the crucial importance of a suitable orientation of the enzyme on the electrode surface.

Funding: This work was supported by French state funds within the framework of the Cluster of Excellence MATISSE led by Sorbonne Université.

References

[1] F. Calle-Vallejo, J. Tymoczko, V. Colic, Q.H. Vu, M.D. Pohl, K. Morgenstern, D. Loffreda, P. Sautet, W. Schuhmann, A.S. Bandarenka, Finding optimal surface sites on heterogeneous catalysts by counting nearest neighbors, Science, 350 (2015) 185-189.

[2] A.T. Yahiro, S.M. Lee, D.O. Kimble, Bioelectrochemistry: I. Enzyme utilizing bio-fuel cell studies, Biochimica et Biophysica Acta (BBA) - Specialized Section on Biophysical Subjects, 88 (1964) 375-383.

[3] B. Olszewski, K. Stolarczyk, Laccase-Catalyzed Reduction of Oxygen at Electrodes Modified by Carbon Nanotubes with Adsorbed Promazine or Acetosyringone, Catalysts, 8 (2018) 414.

[4] N. Mano, A. de Poulpiquet, O2 Reduction in Enzymatic Biofuel Cells, Chemical Reviews, 118 (2018) 2392-2468.

[5] X. Huang, L. Zhang, Z. Zhang, S. Guo, H. Shang, Y. Li, J. Liu, Wearable biofuel cells based on the classification of enzyme for high power outputs and lifetimes, Biosensors and Bioelectronics, 124-125 (2019) 40-52.

[6] A.J. Bandodkar, Review—Wearable Biofuel Cells: Past, Present and Future, Journal of The Electrochemical Society, 164 (2017) H3007-H3014.

[7] S. Shleev, Quo Vadis, Implanted Fuel Cell?, ChemPlusChem, 82 (2017) 522-539.

[8] C.-e. Zhao, P. Gai, R. Song, Y. Chen, J. Zhang, J.-J. Zhu, Nanostructured material-based biofuel cells: recent advances and future prospects, Chemical Society Reviews, 46 (2017) 1545-1564.

[9] S. Cosnier, A.J. Gross, F. Giroud, M. Holzinger, Beyond the hype surrounding biofuel cells: What's the future of enzymatic fuel cells?, Current Opinion in Electrochemistry, 12 (2018) 148-155.

[10] L. Rajendran, M. Kirthiga, E. Laborda, Mathematical modeling of nonlinear reaction–diffusion processes in enzymatic biofuel cells, Current Opinion in Electrochemistry, 1 (2017) 121-132.

[11] Y. Holade, S. Tingry, K. Servat, T.W. Napporn, D. Cornu, K.B. Kokoh, Nanostructured Inorganic Materials at Work in Electrochemical Sensing and Biofuel Cells, Catalysts, 7 (2017) 31.

[12] I. Mazurenko, X. Wang, A. de Poulpiquet, E. Lojou, H2/O2 enzymatic fuel cells: from proof-of-concept to powerful devices, Sustainable Energy & Fuels, 1 (2017) 1475-1501.

[13] X. Xiao, H.-q. Xia, R. Wu, L. Bai, L. Yan, E. Magner, S. Cosnier, E. Lojou, Z. Zhu, A. Liu, Tackling the Challenges of Enzymatic (Bio)Fuel Cells, Chemical Reviews, 119 (2019) 9509–9558.

[14] A. Nasar, R. Perveen, Applications of enzymatic biofuel cells in bioelectronic devices – A review, International Journal of Hydrogen Energy, 44 (2019) 15287-15312.

[15] J. Tang, X. Yan, C. Engelbrekt, J. Ulstrup, E. Magner, X. Xiao, J. Zhang, Development of graphene-based enzymatic biofuel cells: A minireview, Bioelectrochemistry, 134 (2020) 107537.

[16] Q. Xu, F. Zhang, L. Xu, P. Leung, C. Yang, H. Li, The applications and prospect of fuel cells in medical field: A review, Renewable and Sustainable Energy Reviews, 67 (2017) 574-580.

[17] A.A. Babadi, S. Bagheri, S.Bee A. Hamid, Progress on implantable biofuel cell: Nano-carbon functionalization for enzyme immobilization enhancement, Biosensors and Bioelectronics, 79 (2016) 850-860.

[18] S. Cosnier, A. Le Goff, M. Holzinger, Towards glucose biofuel cells implanted in human body for powering artificial organs: Review, Electrochemistry Communications, 38 (2014) 19-23.

[19] M. Southcott, K. MacVittie, J. Halamek, L. Halamkova, W.D. Jemison, R. Lobel, E. Katz, A pacemaker powered by an implantable biofuel cell operating under conditions mimicking the human blood circulatory system - battery not included, Physical Chemistry Chemical Physics, 15 (2013) 6278-6283.

[20] P. Cinquin, C. Gondran, Fabien Giroud, Simon Mazabrard, Aymeric Pellissier, Francis Boucher, Jean-Pierre Alcaraz, Karine Gorgy, F. Lenouvel, S. Mathe, P. Porcu, S. Cosnier, A Glucose BioFuel Cell Implanted in Rats, PloS One, 5 (2010) e10476.

[21] A.J. Bandodkar, J.-M. You, N.-H. Kim, Y. Gu, R. Kumar, A.M.V. Mohan, J. Kurniawan, S. Imani, T. Nakagawa, B. Parish, M. Parthasarathy, P.P. Mercier, S. Xu, J. Wang, Soft, stretchable, high power density electronic skin-based biofuel cells for scavenging energy from human sweat, Energy & Environmental Science, 10 (2017) 1581-1589.

[22] C. Abreu, Y. Nedellec, O. Ondel, F. Buret, S. Cosnier, A. Le Goff, M. Holzinger, Towards eco-friendly power sources: In series connected glucose biofuel cells power a disposable ovulation test, Sensors and Actuators B: Chemical, 277 (2018) 360-364.
[23] Y. Chen, P. Gai, J. Zhang, J.-J. Zhu, Design of an enzymatic biofuel cell with large power output, Journal of Materials Chemistry A, 3 (2015) 11511-11516.
[24] H. Sakai, T. Nakagawa, Y. Tokita, T. Hatazawa, T. Ikeda, S. Tsujimura, K. Kano, A high-power glucose/oxygen biofuel cell operating under quiescent conditions, Energy & Environmental Science, 2 (2009) 133-138.
[25] K. Saravanakumar, S.P. Ganesan, L. Rajendran, Theoretical Analysis of Reaction and Diffusion Processes in a Biofuel Cell Electrode, Fuel Cells, (2015) n/a-n/a.
[26] H. Zhang, L. Zhang, Y. Han, Y. Yu, M. Xu, X. Zhang, L. Huang, S. Dong, RGO/Au NPs/N-doped CNTs supported on nickel foam as an anode for enzymatic biofuel cells, Biosensors and Bioelectronics, 97 (2017) 34-40.
[27] F. Shen, D. Pankratov, G. Pankratova, M.D. Toscano, J. Zhang, J. Ulstrup, Q. Chi, L. Gorton, Supercapacitor/biofuel cell hybrid device employing biomolecules for energy conversion and charge storage, Bioelectrochemistry, 128 (2019) 94-99.
[28] N.A. Daronch, M. Kelbert, C.S. Pereira, P.H.H. de Araújo, D. de Oliveira, Elucidating the choice for a precise matrix for laccase immobilization: A review, Chemical Engineering Journal, 397 (2020) 125506.
[29] V.A. Bogdanovskaya, I.N. Arkad'eva, M.A. Osina, Bioelectrocatalytic Oxygen Reduction by Laccase Immobilized on Various Carbon Carriers, Russian Journal of Electrochemistry, 53 (2017) 1323-1333.
[30] D. Majdecka, R. Bilewicz, Nanostructuring carbon supports for optimal electrode performance in biofuel cells and hybrid fuel cells, J Solid State Electrochem, 20 (2016) 949-955.
[31] P. Jenkins, S. Tuurala, A. Vaari, M. Valkiainen, M. Smolander, D. Leech, A mediated glucose/oxygen enzymatic fuel cell based on printed carbon inks containing aldose dehydrogenase and laccase as anode and cathode, Enzyme and Microbial Technology, 50 (2012) 181-187.
[32] V. Wernert, C. Lebouin, V. Benoit, R. Gadiou, A. de Poulpiquet, E. Lojou, R. Denoyel, Direct electron transfer of bilirubin oxidase at a carbon flow-through electrode, Electrochimica Acta, 283 (2018) 88-96.
[33] T. Yoon, I. Baek, S. Lee, H. Choi, S. Yoon, H. Lee, S. Ung Kim, S. Na, Immobilization of laccase on a graphene interface: Direct electron transfer and molecular dynamics study, Applied Surface Science, 521 (2020) 146378.
[34] J. Filip, J. Tkac, Is graphene worth using in biofuel cells?, Electrochimica Acta, 136 (2014) 340-354.
[35] C. Di Bari, A. Goñi-Urtiaga, M. Pita, S. Shleev, M.D. Toscano, R. Sainz, A.L. De Lacey, Fabrication of high surface area graphene electrodes with high performance towards enzymatic oxygen reduction, Electrochimica Acta, 191 (2016) 500-509.
[36] M. Holzinger, A. Le Goff, S. Cosnier, Carbon nanotube/enzyme biofuel cells, Electrochimica Acta, 82 (2012) 179-190.
[37] H.-q. Xia, Y. Kitazumi, O. Shirai, H. Ozawa, M. Onizuka, T. Komukai, K. Kano, Factors affecting the interaction between carbon nanotubes and redox enzymes in direct electron transfer-type bioelectrocatalysis, Bioelectrochemistry, 118 (2017) 70-74.
[38] O. Fokina, J. Eipper, L. Winandy, S. Kerzenmacher, R. Fischer, Improving the performance of a biofuel cell cathode with laccase-containing culture supernatant from Pycnoporus sanguineus, Bioresource Technology, 175 (2015) 445-453.
[39] L. Hussein, S. Rubenwolf, F. von Stetten, G. Urban, R. Zengerle, M. Krueger, S. Kerzenmacher, A highly efficient buckypaper-based electrode material for mediatorless laccase-catalyzed dioxygen reduction, Biosensors and Bioelectronics, 26 (2011) 4133-4138.
[40] R.P. Ramasamy, H.R. Luckarift, D.M. Ivnitski, P.B. Atanassov, G.R. Johnson, High electrocatalytic activity of tethered multicopper oxidase–carbon nanotube conjugates, Chemical Communications, 46 (2010) 6045-6047.

[41] C. Tortolini, S. Rea, E. Carota, S. Cannistraro, F. Mazzei, Influence of the immobilization procedures on the electroanalytical performances of Trametes versicolor laccase based bioelectrode, Microchemical Journal, 100 (2011) 8-13.
[42] C.H. Kwon, J.A. Lee, Y.-B. Choi, H.-H. Kim, G.M. Spinks, M.D. Lima, R.H. Baughman, S.J. Kim, Stability of carbon nanotube yarn biofuel cell in human body fluid, Journal of Power Sources, 286 (2015) 103-108.
[43] A. Zebda, Chantal Gondran, Alan Le Goff, Michael Holzinger, P. Cinquin, S. Cosnier, Mediatorless high-power glucose biofuel cells based on compressed carbon nanotube-enzyme electrodes, nature communication, (2011).
[44] B. Reuillard, A. Le Goff, C. Agnès, A. Zebda, M. Holzinger, S. Cosnier, Direct electron transfer between tyrosinase and multi-walled carbon nanotubes for bioelectrocatalytic oxygen reduction, Electrochemistry Communications, 20 (2012) 19-22.
[45] K. Davami, M. Shaygan, N. Kheirabi, J. Zhao, D.A. Kovalenko, M.H. Rümmeli, J. Opitz, G. Cuniberti, J.-S. Lee, M. Meyyappan, Synthesis and characterization of carbon nanowalls on different substrates by radio frequency plasma enhanced chemical vapor deposition, Carbon, 72 (2014) 372-380.
[46] S. Mori, T. Ueno, M. Suzuki, Synthesis of carbon nanowalls by plasma-enhanced chemical vapor deposition in a CO/H2 microwave discharge system, Diamond and Related Materials, 20 (2011) 1129-1132.
[47] K. Ostrikov, E.C. Neyts, M. Meyyappan, Plasma nanoscience: from nano-solids in plasmas to nano-plasmas in solids, Advances in Physics, 62 (2013) 113-224.
[48] J. Yao, Y. Huang, Y. Hou, B. Yang, L. Lei, X. Tang, K.G. Scheckel, Z. Li, D. Wu, D.D. Dionysiou, Graphene-modified graphite paper cathode for the efficient bioelectrochemical removal of chromium, Chemical Engineering Journal, 405 (2021) 126545.
[49] S.A. Evlashin, Y.M. Maksimov, P.V. Dyakonov, A.A. Pilevsky, K.I. Maslakov, Y.A. Mankelevich, E.N. Voronina, S.V. Vavilov, A.A. Pavlov, E.V. Zenova, I.S. Akhatov, N.V. Suetin, N-Doped Carbon NanoWalls for Power Sources, Sci Rep, 9 (2019) 6716-6716.
[50] M. Taniguchi, R. Yoshie, K. Akikubo, A. Tateno, K. Hotozuka, N. Kawaguchi, T. Uchida, M. Tanimura, M. Tachibana, Effect of nitrogen and iron in carbon nanowalls on oxygen reduction reaction, Electrochimica Acta, 306 (2019) 132-142.
[51] A. Korani, A. Salimi, High performance glucose/O2 compartment-less biofuel cell using DNA/CNTs as platform for immobilizing bilirubin oxidase as novel biocathode and integrated NH2-CNTs/dendrimer/glucose dehydrogenase/nile blue as bioanode, Electrochimica Acta, 185 (2015) 90-100.
[52] N. Lalaoui, R. David, H. Jamet, M. Holzinger, A. Le Goff, S. Cosnier, Hosting Adamantane in the Substrate Pocket of Laccase: Direct Bioelectrocatalytic Reduction of O2 on Functionalized Carbon Nanotubes, ACS Catal., 6 (2016) 4259-4264.
[53] N. Lalaoui, M. Holzinger, A. Le Goff, S. Cosnier, Diazonium Functionalisation of Carbon Nanotubes for Specific Orientation of Multicopper Oxidases: Controlling Electron Entry Points and Oxygen Diffusion to the Enzyme, Chem. - Eur. J., 22 (2016) 10494-10500.
[54] F. Gouranlou, H. Ghourchian, Ethanol/O2 biofuel cell using a biocathode consisting of laccase/ HOOC-MWCNTs/polydiallyldimethylammonium chloride, Enzyme and Microbial Technology, 86 (2016) 127-133.
[55] F.-H. Kuok, H.-H. Chien, C.-C. Lee, Y.-C. Hao, I.-S. Yu, C.-C. Hsu, I.C. Cheng, J.-Z. Chen, Atmospheric-pressure-plasma-jet processed carbon nanotube (CNT)-reduced graphene oxide (rGO) nanocomposites for gel-electrolyte supercapacitors, RSC Adv., 8 (2018) 2851-2857.
[56] F.-H. Kuok, K.-Y. Kan, I.-S. Yu, C.-W. Chen, C.-C. Hsu, I.C. Cheng, J.-Z. Chen, Application of atmospheric-pressure plasma jet processed carbon nanotubes to liquid and quasi-solid-state gel electrolyte supercapacitors, Appl. Surf. Sci., 425 (2017) 321-328.
[57] B.-J. Lee, G.-H. Jeong, Efficient surface functionalization of vertically-aligned carbon nanotube arrays using an atmospheric pressure plasma jet system, Fullerenes, Nanotubes, Carbon Nanostruct., 20 (2018) 116-122.

[58] D. Kolacyak, J. Ihde, C. Merten, A. Hartwig, U. Lommatzsch, Fast functionalization of multi-walled carbon nanotubes by an atmospheric pressure plasma jet, Journal of Colloid and Interface Science, 359 (2011) 311-317.
[59] T. Abuzairi, M. Okada, R.W. Purnamaningsih, N.R. Poespawati, F. Iwata, M. Nagatsu, Maskless localized patterning of biomolecules on carbon nanotube microarray functionalized by ultrafine atmospheric pressure plasma jet using biotin-avidin system, Appl. Phys. Lett., 109 (2016) 023701/023701-023701/023704.
[60] M. Ardhaoui, M. Zheng, J. Pulpytel, D. Dowling, C. Jolivalt, F.A. Khonsari, Plasma functionalized carbon electrode for laccase-catalyzed oxygen reduction by direct electron transfer, Bioelectrochemistry, 91 (2013) 52-61.
[61] H.B. Gray, J.R. Winkler, Electron flow through metalloproteins, Biochimica et Biophysica Acta (BBA) - Bioenergetics, 1797 (2010) 1563-1572.
[62] V.P. Hitaishi, R. Clement, N. Bourassin, M. Baaden, A. De Poulpiquet, S. Sacquin-Mora, A. Ciaccafava, E. Lojou, Controlling Redox Enzyme Orientation at Planar Electrodes, Catalysts, 8 (2018) 192.
[63] V.P. Hitaishi, R. Clément, L. Quattrocchi, P. Parent, D. Duché, L. Zuily, M. Ilbert, E. Lojou, I. Mazurenko, Interplay between Orientation at Electrodes and Copper Activation of Thermus thermophilus Laccase for O2 Reduction, Journal of the American Chemical Society, (2019).
[64] Y. Sugimoto, K. So, H.Q. Xia, K. Kano, Orientation-Oriented Adsorption and Immobilization of Redox Enzymes for Electrochemical Communication With Electrodes, in: K. Wandelt (Ed.) Encyclopedia of Interfacial Chemistry, Elsevier, Oxford, 2018, pp. 403-421.
[65] A. Blout, F. Billon, C. Calers, C. Méthivier, A. Pailleret, H. Perrot, C. Jolivalt, Orientation of a Trametes versicolor laccase on amorphous carbon nitride coated graphite electrodes for improved electroreduction of dioxygen to water, Electrochimica Acta, 277 (2018) 255-267.
[66] J. Tang, X. Yan, W. Huang, C. Engelbrekt, J.Ø. Duus, J. Ulstrup, X. Xiao, J. Zhang, Bilirubin oxidase oriented on novel type three-dimensional biocathodes with reduced graphene aggregation for biocathode, Biosensors and Bioelectronics, 167 (2020) 112500.
[67] N. Lalaoui, K. Elouarzaki, A.L. Goff, M. Holzinger, S. Cosnier, Efficient direct oxygen reduction by laccases attached and oriented on pyrene-functionalized polypyrrole/carbon nanotube electrodes, Chemical Communications, 49 (2013) 9281-9283.
[68] S. Babanova, K. Artyushkova, Y. Ulyanova, S. Singhal, P. Atanassov, Design of experiments and principal component analysis as approaches for enhancing performance of gas-diffusional air-breathing bilirubin oxidase cathode, Journal of Power Sources, 245 (2014) 389-397.
[69] Thomas Bertrand, Claude Jolivalt, Eliane Caminade, Nathalie Joly, Christian Mouginb, Pierre Briozzoc, Purification and preliminary crystallographic study of Trametes versicolor laccase in its native form, Acta Crystallographia Section D, (2001).
[70] D. Montgomery, Design and Analysis of Experiments, 8th ed., John Wiley & Sons2012.
[71] G.E.P. Box, K.B. Wilson, On the Experimental Attainment of Optimum Conditions, Journal of the Royal Statistical Society. Series B (Methodological), 13 (1951) 1-45.
[72] G.T. Hermanson, Chapter 20 - Antibody Modification and Conjugation, in: G.T. Hermanson (Ed.) Bioconjugate Techniques (Third Edition), Academic Press, Boston, 2013, pp. 867-920.
[73] D. BRIGGS, M.P. SEAH, Practical surface analysis, John WILLEY & SONS, 1 (1993).
[74] J. Pinson, F. Podvorica, Attachment of organic layers to conductive or semiconductive surfaces by reduction of diazonium salts, Chemical Society Reviews, 34 (2005) 429-439.
[75] C. Gutiérrez-Sánchez, M. Pita, C. Vaz-Domínguez, S. Shleev, A.L. De Lacey, Gold Nanoparticles as Electronic Bridges for Laccase-Based Biocathodes, Journal of the American Chemical Society, 134 (2012) 17212-17220.
[76] T. Bertrand, C. Jolivalt, P. Briozzo, E. Caminade, N. Joly, C. Madzak, C. Mougin, Crystal Structure of a Four-Copper Laccase Complexed with an Arylamine: Insights into Substrate Recognition and Correlation with Kinetics†,‡, Biochemistry, 41 (2002) 7325-7333.
[77] J. Káš, J. Sajdok, F. Strejček, Immunoaffinity chromatography and oriented immobilisation of antibodies, Immobilised Macromolecules: Application Potentials, Springer1993, pp. 37-49.

[78] O. El-Mahdi, O. Melnyk, α-Oxo Aldehyde or Glyoxylyl Group Chemistry in Peptide Bioconjugation, Bioconjugate Chemistry, 24 (2012) 735-765.
[79] G. Chaga, A general method for immobilization of glycoproteins on regenerable immobilized metal-ion carriers: application to glucose oxidase from Penicillium chrysogenum and horseradish peroxidase, Biotechnology and applied biochemistry 20 (1994) 43-53.
[80] N. Lalaoui, P. Rousselot-Pailley, V. Robert, Y. Mekmouche, R. Villalonga, M. Holzinger, S. Cosnier, T. Tron, A. Le Goff, Direct Electron Transfer between a Site-Specific Pyrene-Modified Laccase and Carbon Nanotube/Gold Nanoparticle Supramolecular Assemblies for Bioelectrocatalytic Dioxygen Reduction, ACS Catalysis, 6 (2016) 1894-1900.
[81] F. Giroud, R.D. Milton, B.-X. Tan, S.D. Minteer, Simplifying Enzymatic Biofuel Cells: Immobilized Naphthoquinone as a Biocathodic Orientational Moiety and Bioanodic Electron Mediator, ACS Catalysis, 5 (2015) 1240-1244.
[82] M. Kizling, S. Draminska, K. Stolarczyk, P. Tammela, Z. Wang, L. Nyholm, R. Bilewicz, Biosupercapacitors for powering oxygen sensing devices, Bioelectrochemistry, 106 (2015) 34-40.
[83] C.C. Dupont-Gillain, I. Jacquemart, Patterned collagen layers on polystyrene: direct probing using AFM in the adhesion mapping mode, Surface science, 539 (2003) 145-154.
[84] T. Bertrand, C. Jolivalt, P. Briozzo, E. Caminade, N. Joly, C. Madzak, C. Mougin, Crystal Structure of a Four-Copper Laccase Complexed with an Arylamine: Insights into Substrate Recognition and Correlation with Kinetics, Biochemistry, 41 (2002) 7325-7333.
[85] T. Bertrand, C. Jolivalt, E. Caminade, N. Joly, C. Mougin, P. Briozzo, Purification and preliminary crystallographic study of Trametes versicolor laccase in its native form, Acta Crystallographica Section D, 58 (2002) 319-321.

Figure Captions

Figure 1. Schematic of the APPJ setup (left) and picture of the plasma jet (right)

Figure 2. Photograph and schematic of the biocathodes developed in this work

Figure 3. C1s XPS spectra for untreated graphite and graphite after APPJ treatment. APPJ treatment conditions: one cycle, distance nozzle/substrate 1 cm, Nitrogen flow 2000 $L.h^{-1}$, line speed 10 $m.min^{-1}$, PCT 80 %, pulse frequency 21 kHz.

Figure 4. Evolution of the contact angle with the distance between the torch nozzle and the substrate

Figure 5. Evolution of the biocathode current density as a function of the water contact angle according to the results of the Fractional Factorial Design and of the Central Composite Design. The regression curve is obtained with a value of $R^2 = 0.719$.

Figure 6. Contour plot of the biocathode current density calculated from the second order model and a CCD. The experimental results of the reduction current density at 0.2 V/SCE (in $\mu A/cm^2$) are also given in blue. Note that the model extrapolated outside the experimental domain delimited by a circle may not be correct.

Figure 7. Cl2p XPS spectrum of plasma treated graphite after reaction with 2-chlorobenzoic hydrazide.

Figure 8. SEM images of carbon nanowalls deposited by plasma on graphite discs depending on the treatment time (a) 30 s; (b) 60 s; (c and d) 120 s. Scale bars indicate 1 µm.

Figure 9. C1s XPS spectra of graphite@CNW120s treated a) before APPJ treatment, b) after APPJ treatment (d=1 cm and V= 10 $m.min^{-1}$) without laccase and c) after the same APPJ treatment with laccase immobilization by EDC/NHS

Figure 10. Dioxygen reduction current densities on graphite@CNWs120s biocathodes with unmodified and oxidized laccase, with or without coupling agent (EDC/NHS) and for soft (d = 1.5 cm, V = 20 m/min) or strong (d = 1 cm, V = 10 m/min) plasma treatment conditions.

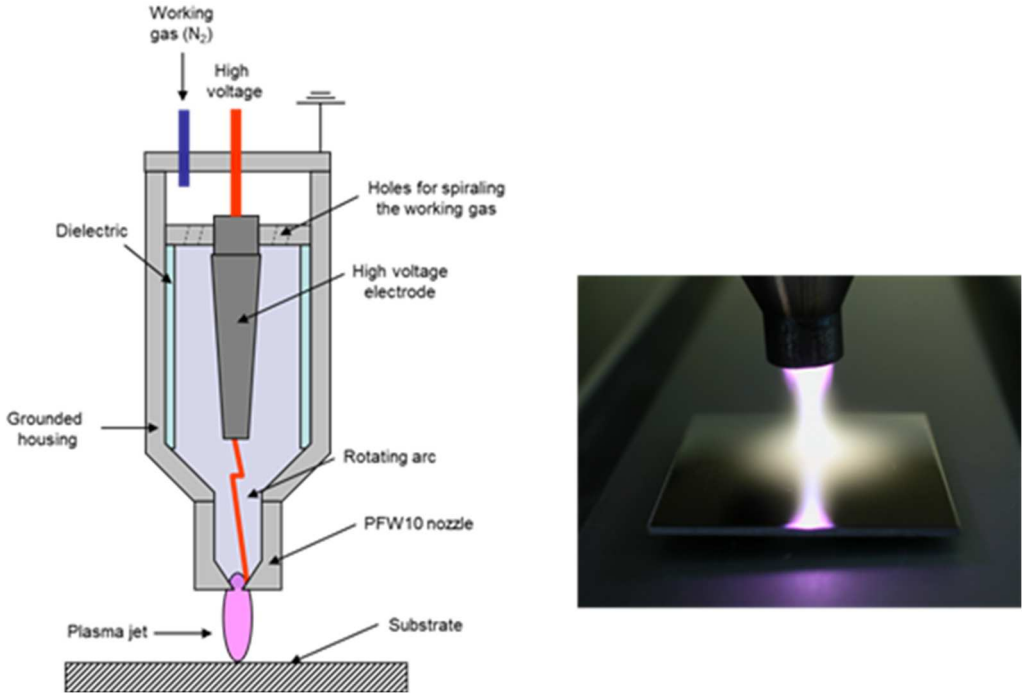

Figure 1. Schematic of the APPJ setup (left) and picture of the plasma jet (right)

Figure 2. Photograph and schematic of the biocathodes developed in this work

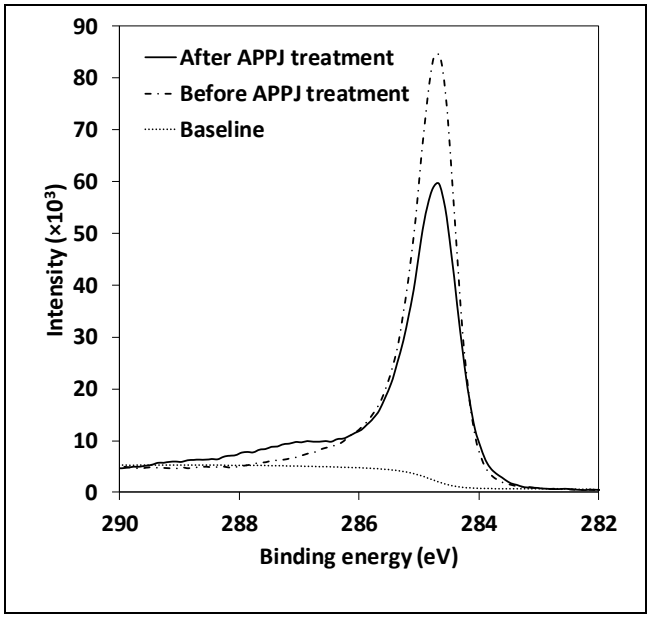

Figure 3. C1s XPS spectra for untreated graphite and graphite after APPJ treatment. APPJ treatment conditions: one cycle, distance nozzle/substrate 1 cm, Nitrogen flow 2000 $L.h^{-1}$, line speed 10 $m.min^{-1}$, PCT 80 %, pulse frequency 21 kHz.

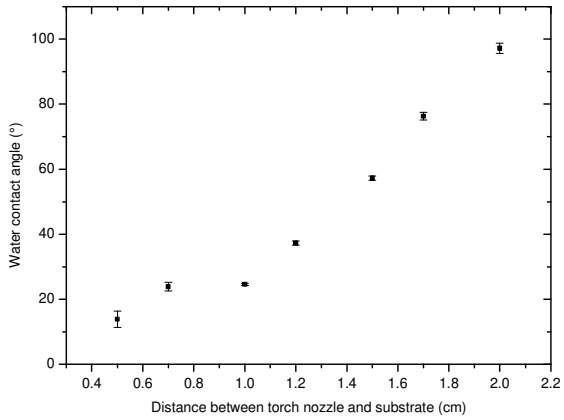

Figure 4. Evolution of the contact angle with the distance between the torch nozzle and the substrate

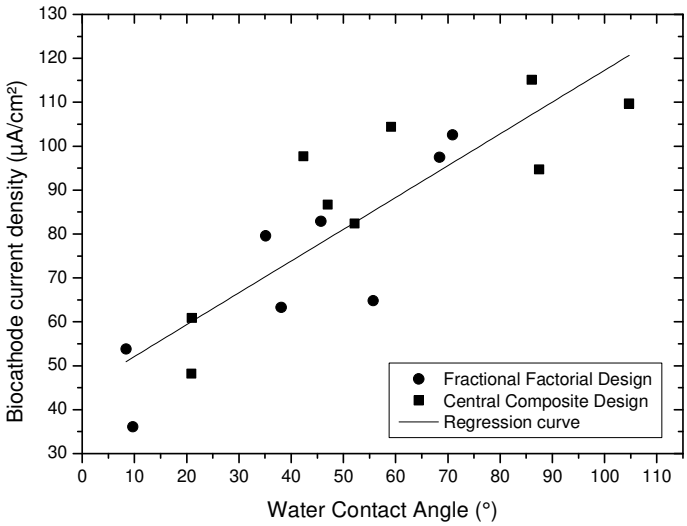

Figure 5. Evolution of the biocathode current density as a function of the water contact angle according to the results of the Fractional Factorial Design and of the Central Composite Design. The regression curve is obtained with a value of $R^2 = 0.719$.

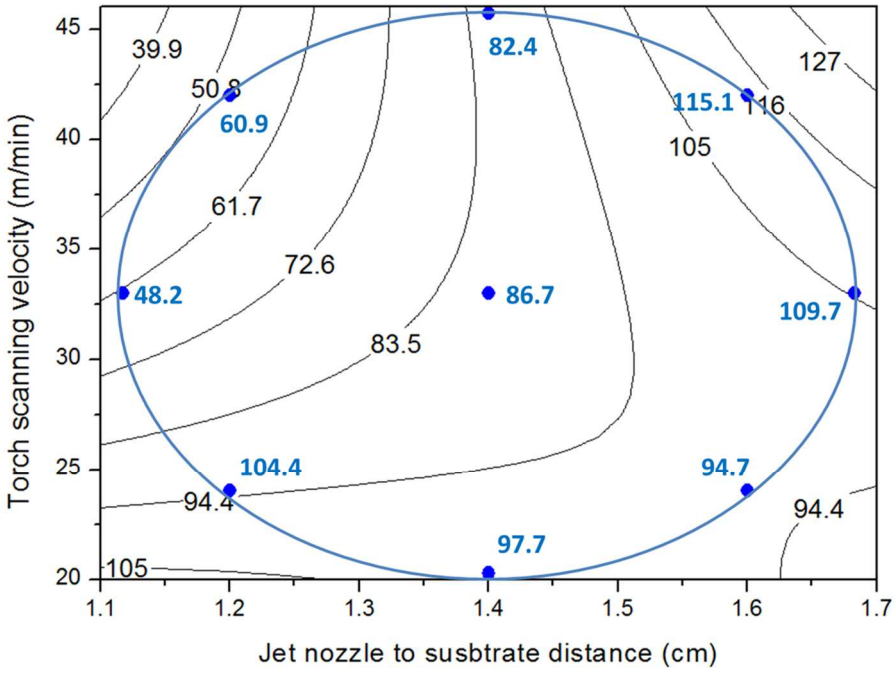

Figure 6. Contour plot of the biocathode current density calculated from the second order model and a CCD. The experimental results of the reduction current density at 0.2 V/SCE (in $\mu A/cm^2$) are also given in blue. Note that the model extrapolated outside the experimental domain delimited by a circle may not be correct.

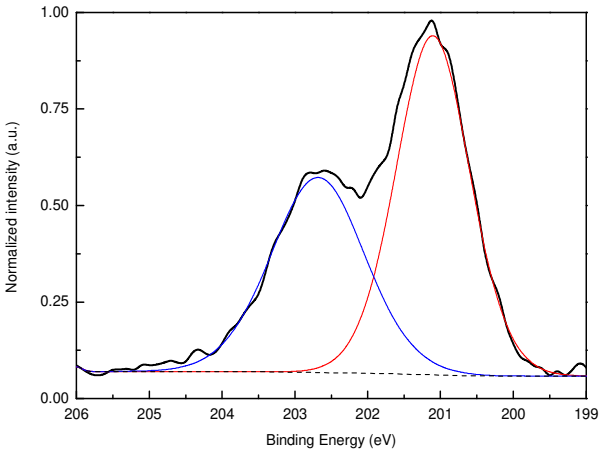

Figure 7. Cl2p XPS spectrum of plasma treated graphite after reaction with 2-chlorobenzoic hydrazide.

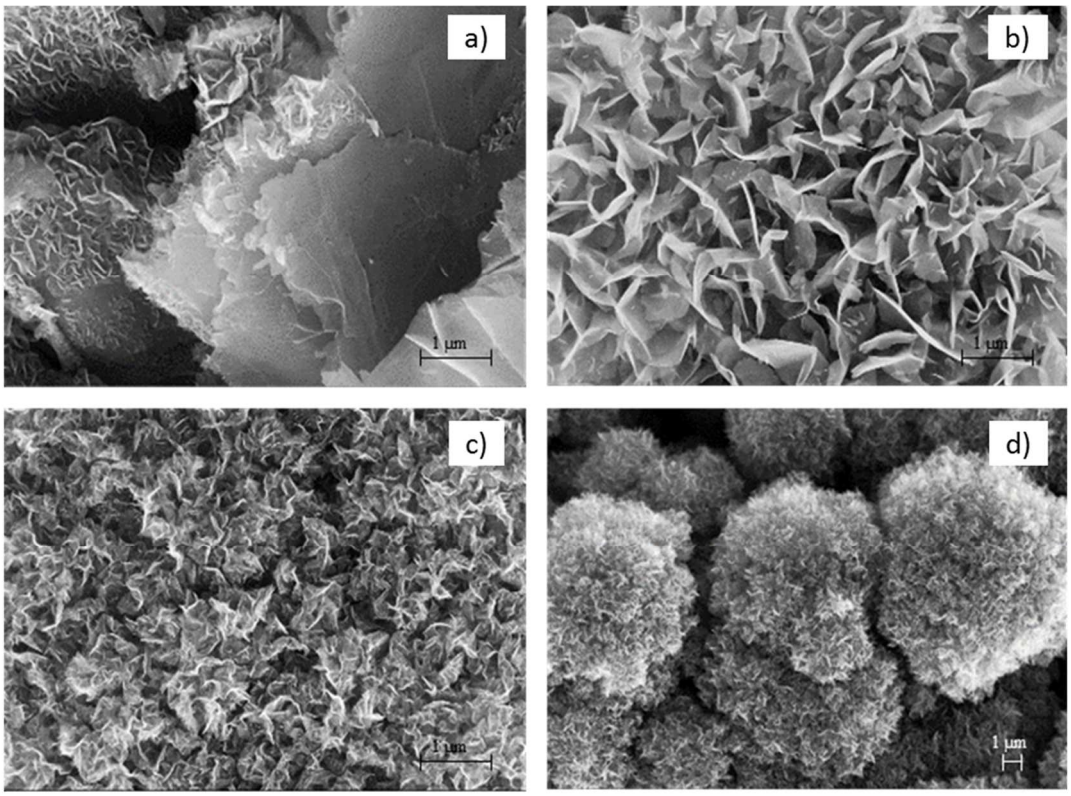

Figure 8. SEM images of carbon nanowalls deposited by plasma on graphite discs depending on the treatment time (a) 30 s; (b) 60 s; (c and d) 120 s; scale bars indicate 1 µm

A B

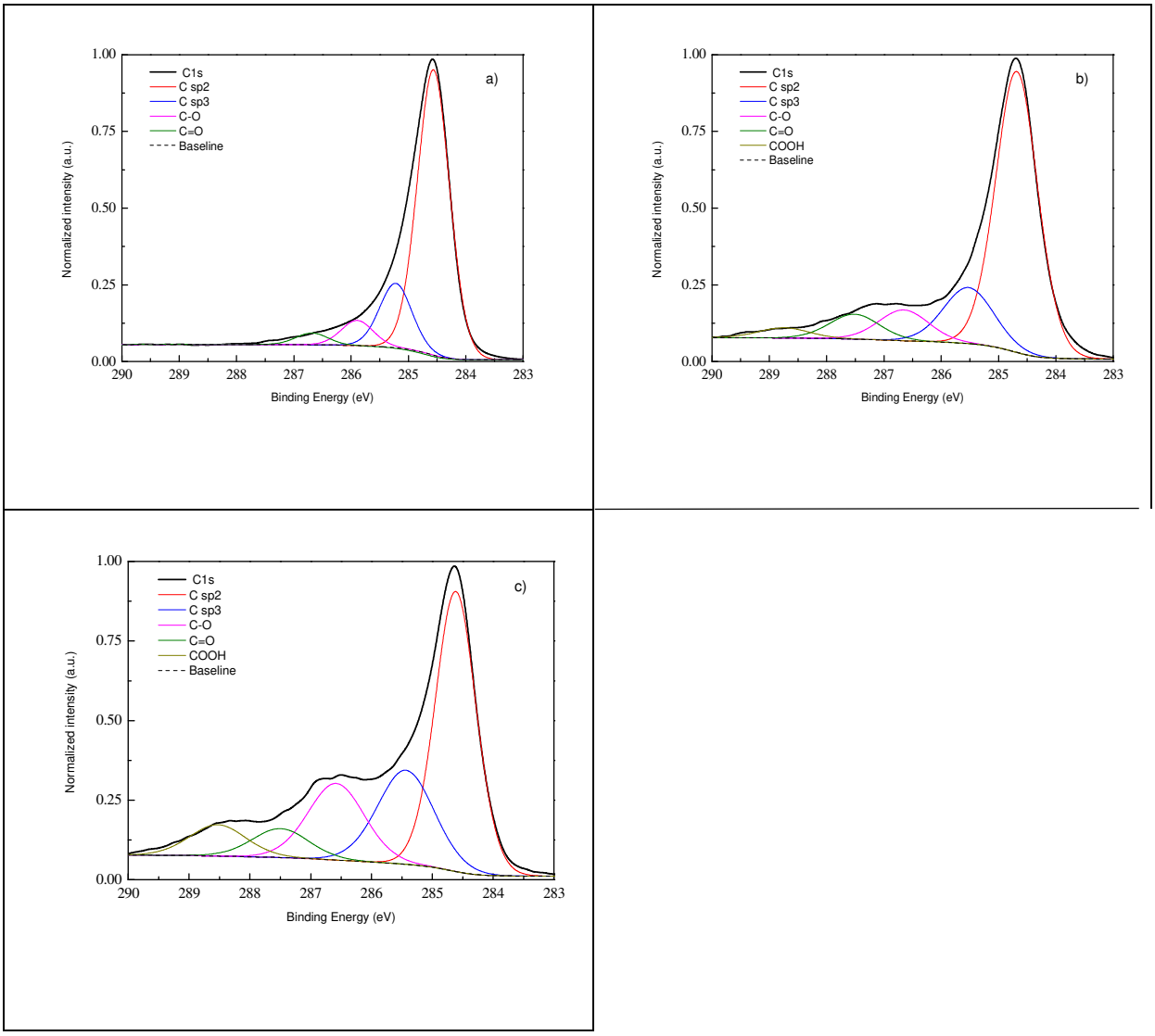

Figure 9. C1s XPS spectra of graphite@CNW120s treated a) before APPJ treatment, b) after APPJ treatment (d=1 cm and V= 10 m.min^{-1}) without laccase and c) after the same APPJ treatment with laccase immobilization by EDC/NHS

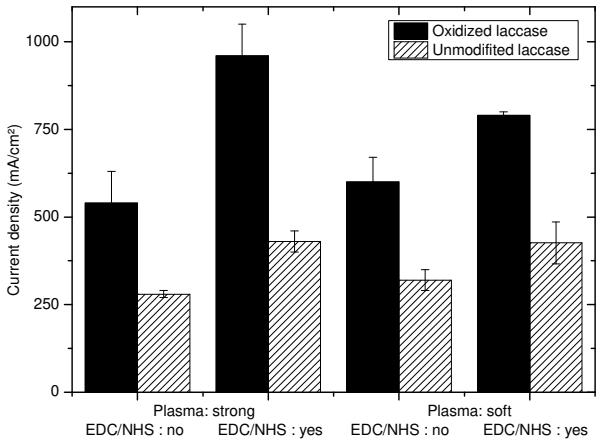

Figure 10. Dioxygen reduction current densities on graphite@CNWs120s biocathodes with unmodified and oxidized laccase, with or without coupling agent (EDC/NHS) and for soft (d = 1.5 cm, V = 20 m/min) or strong (d = 1 cm, V = 10 m/min) plasma treatment conditions.

1. Atmospheric pressure plasma jet functionalisation

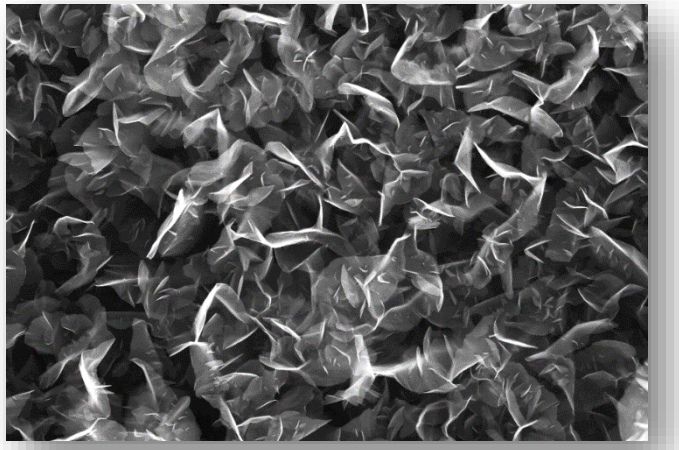

Carbon nanowalls on graphite

2. Laccase grafting

Biocatalytic cathodic current